Altering DNA Polymerase Incorporation Fidelity by Distorting the dNTP Binding Pocket with a Bulky Carcinogen-Damaged Template†

S. Frank Yan,[#,‡] Min Wu,[#] Nicholas E. Geacintov,*[,#] and Suse Broyde*[,§]

Departments of Chemistry and Biology, New York University, New York, New York 10003

Received January 6, 2004; Revised Manuscript Received March 30, 2004

ABSTRACT: Fidelity of DNA polymerases is predominantly governed by an induced fit mechanism in which the incoming dNTP in the ternary complex fits tightly into a binding pocket whose geometry is determined by the nature of the templating base. However, modification of the template with a bulky carcinogen may alter the dNTP binding pocket and thereby the polymerase incorporation fidelity. High fidelity DNA polymerases, such as bacteriophage T7 DNA polymerase, are predominantly blocked by bulky chemical lesions on the template strand during DNA replication. However, some mutagenic bypass can occur, which may lead to carcinogenesis. Experimental studies have shown that a DNA covalent adduct derived from (+)-*anti*-BPDE [(+)-(7*R*,8*S*,9*S*,10*R*)-7,8-dihydroxy-9,10-epoxy-7,8,9,10-tetrahydrobenzo[*a*]pyrene], a carcinogenic metabolite of benzo[*a*]pyrene (BP), primarily blocks Sequenase 2.0, an *exo*$^-$ T7 DNA polymerase; however, a mismatched dATP can be preferentially inserted opposite the damaged adenine templating base within the active site of the polymerase [Chary, P., and Lloyd, R. S. (1995) *Nucleic Acids Res. 23,* 1398−1405]. The goal of this work is to elucidate structural features that contribute to DNA polymerase incorporation fidelity in the presence of this bulky covalent adduct and to interpret the experimental findings on a molecular level. We have carried out molecular modeling and molecular dynamics simulations with AMBER 6.0, investigating a T7 DNA polymerase primer−template closed ternary complex containing this 10*S* (+)-*trans*-*anti*-[BP]-N^6-dA adduct in the templating position within the polymerase active site. All four incoming dNTPs were studied. The simulations show that the BP ring system fits well into an open pocket on the major groove side of the modified template adenine with *anti* glycosidic bond conformation, without disturbing critical polymerase−DNA interactions. However, steric hindrance between the BP ring system and the primer−template DNA causes displacement of the modified template adenine, so that the dNTP base binding pocket is enlarged. This alteration can explain the experimentally observed preference for incorporation of dATP opposite this lesion. These studies also rationalize the observed lower probabilities of incorporation of the other three nucleotides. Our results suggest that the differences in incorporation of dGTP, dCTP, and dTTP are due to the effects of imperfect geometric complementarity. Thus, the simulations suggest that altered DNA polymerase incorporation fidelity can result from adduct-induced changes in the dNTP base binding pocket geometry. Furthermore, plausible structural explanations for the observed effects of [BP]-N^6-dA adduct stereochemistry on the observed stalling patterns are proposed.

DNA[1] replication fidelity is of pivotal importance in maintaining genomic integrity. X-ray crystal structures (*1*, *2*) and kinetic studies (*3*−*7*) of various DNA polymerases suggest that high nucleotide incorporation fidelity is achieved through geometric selection (*7*) and an induced fit mechanism which prevents nucleotide misincorporation (*7*−*9*). The dNTP binding pocket (defined by the polymerase residues as well as the DNA bases) snugly accommodates only the correctly inserted dNTP in the ternary complex containing polymerase, primer−template, and incoming dNTP. Current understanding of polymerase mechanisms suggests that at least three separate steps are involved in achieving faithful incorporation, namely, initial dNTP binding, a conformational change of the polymerase from an "open" to a "closed" state, and the formation of the new phosphodiester bond (*6*, *7*). Crystal structures of open (binary complex) and closed (ternary complex) polymerase structures (*1*, *2*, *10*−*20*) led to the suggestion that the conformational change from the "open" to the "closed" state induced by dNTP binding is a slow step (*10*). Recent work indicates that the "chemistry step" resulting in the formation of the phosphodiester bond may be slow or rate-limiting (*21*, *22*), while the conforma-

† This research is supported by NIH Grant CA-28038 to S.B. and NIH Grant CA-099194 to N.E.G.

* To whom correspondence should be addressed. (N.E.G.) Telephone: 212-998-8407. Fax: 212-998-8421. E-mail: ng1@nyu.edu; (S.B.) Telephone: 212-998-8231. Fax: 212-995-4015. E-mail: broyde@nyu.edu.

[#] Department of Chemistry.

[§] Department of Biology.

[‡] Current address: Genomics Institute of the Novartis Research Foundation, San Diego, CA 92121. E-mail: syan@gnf.org.

[1] Abbreviations: (+)-*anti*-BPDE, (+)-(7*R*,8*S*,9*S*,10*R*)-7,8-dihydroxy-9,10-epoxy-7,8,9,10-tetrahydrobenzo[*a*]pyrene; BP, benzo[*a*]pyrene; BPDE, benzo[*a*]pyrene diol epoxide; DNA, deoxyribonucleic acid; dNTP, deoxynucleoside triphosphate; MD, molecular dynamics; MM, molecular mechanics; NMR, nuclear magnetic resonance; PME, particle mesh Ewald, QM, quantum mechanics; RESP, restrained electrostatic potential fitting; RMSD, root-mean-square deviation.

10.1021/bi0499516 CCC: $27.50
Published on Web 05/27/2004

tional transition may be relatively rapid (*23*−*26*); however, further studies will be needed to delineate the generality of this suggestion for various polymerases. Combined quantum mechanics/molecular mechanics (QM/MM) studies have recently traced the free energy along the reaction coordinate and deduced an activation energy barrier of ∼18 kcal/mol in the chemical step (*22*); this work suggested that the final organization of the transition complex, possibly involving rearrangement of the key active site amino acid residues and the incoming dNTP, is slow. The formation of the transition complex would be expected to be much more difficult in the case of incorrect as compared to correct dNTPs, involving a higher barrier and therefore much slower incorporation rates due to imperfect alignment of the misinserted dNTP. It is suggested that the reaction mechanism for the incorrect dNTP substrates may differ from that occurring in the case of the correct incoming dNTP (*22*). Moreover, protein mutation experiments suggest that DNA replication fidelity can be significantly affected by altering the geometry of the DNA binding pocket through mutations of key protein residues (*27*).

Benzo[*a*]pyrene (BP), a common environmental carcinogen, is present in tobacco smoke, automobile exhaust, and as a contaminant in foods (*28*−*31*). Upon metabolic activation, BP can be converted to highly reactive and mutagenic *syn* and *anti* benzo[*a*]pyrene diol epoxides (BPDEs) (*32*). These *syn* and *anti* BPDEs can react with purines in DNA by *cis* and *trans* epoxide opening to yield covalent adducts (*33*−*35*). The major adenine adducts are the 10*S* (+)- and 10*R* (−)-*trans*-*anti*-[BP]-N^6-dA adducts (*33*−*35*). High-resolution NMR solution studies of BP adenine adducts have shown that the BP moiety is intercalated into the B-DNA double helix, on the 5′-side of the modified adenine in the case of *R* isomers, while *S* isomers are intercalated on the 3′-side (*36*−*42*). During DNA replication, these bulky lesions predominantly block high fidelity DNA polymerases; however, a small fraction of bypass can occur, which may produce mutations that could initiate the process of carcinogenesis (*43*−*46*). Since mutagenic bypass is rare in replicative polymerases, it may involve conformers present in small proportions, which would be difficult to observe experimentally; however, computational approaches can help elucidate structural possibilities in molecular detail, and thereby suggest how such rare but potentially harmful events may occur.

Nucleotide incorporation experiments in vitro have shown that Sequenase 2.0 (an *exo*$^-$ T7 DNA polymerase) inserts mainly dATP opposite the 10*S* (+)-*trans*-*anti*-[BP]-N^6-dA adduct, thus producing A−A mismatches in the polymerase active site. However, smaller amounts of dTTP and dGTP insertions were also observed (*47*). Furthermore, the absolute configuration of the adducts at the C10 position of the BP residue was found to influence the stalling patterns of the polymerase. The 10*S* (+)-*trans*-*anti*-[BP]-N^6-dA adduct blocks the Sequenase 2.0 to a similar extent one base 3′ to the lesion, as well as at the lesion site, while the stereoisomeric 10*R* adduct blocks the polymerase predominantly at the adduct site (*47*). All these results are qualitatively well defined in this work, and hence provide a valuable experimental connection to our modeling study. It should be noted that marked differences were obtained when Sequenase was replaced by other polymerases in this study (*47*), indicating that structural effects of individual polymerases must be individually dissected.

The goal of this work is to elucidate structural features that contribute to DNA polymerase incorporation fidelity in the presence of a bulky lesion, the 10*S* (+)-*trans*-*anti*-[BP]-N^6-dA adduct, with the data of Chary and Lloyd (*47*) as an experimental connection. We are motivated by the hypothesis that observed insertion preferences are structurally guided rather than determined by "A-rule" type of noninstructional dATP incorporation (*48*) as in the case of abasic sites (*49*, *50*). We have carried out computer modeling and molecular dynamics simulations of the T7 DNA polymerase primer−template ternary complex containing a 10*S* (+)-*trans*-*anti*-[BP]-N^6-dA adduct with all four different incoming dNTPs within the polymerase active site. We also carried out a simulation containing an unmodified adenine template with an incoming dTTP as a control. The high-resolution X-ray crystal structure of the "closed" T7 DNA polymerase ternary complex (*51*) and an NMR solution conformation of the 10*S* (+)-*trans*-*anti*-[BP]-N^6-dA adduct (*38*) served as initial structural models. Our results show, on a molecular level, that nucleotide incorporation is determined by the shape and size of the polymerase dNTP base binding pocket, which is largely dictated by the positioning of the templating base. In our simulations, the BP ring system is accommodated in the T7 DNA polymerase complex in the open pocket on the major groove side of the primer−template DNA. However, steric hindrance between the BP moiety and the primer−template DNA causes the modified templating adenine to be displaced away from the active site of the polymerase. This produces an enlargement in the dNTP base binding pocket, which allows the preferred accommodation of the mismatched incoming dATP observed experimentally. Thus, the simulated results show that modification of the templating base can alter DNA polymerase incorporation fidelity by changing the dNTP base binding pocket. Imperfect geometric complementarity involving an enlarged pocket also rationalizes the lesser incorporation of other dNTPs. In addition, the observed blockage patterns of T7 DNA polymerase by the stereoisomeric 10*S* (+)- and 10*R* (−)-*trans*-*anti*-[BP]-N^6-dA adducts is structurally rationalized by modeling.

MATERIALS AND METHODS

Molecular Modeling of the Starting Structures. The crystal structure of the T7 DNA polymerase ternary complex (*51*) obtained from the Protein Data Bank (*52*) (PDB ID: 1T7P) served as the starting structure for our modeling. The missing residues and loops in the original crystal structure, namely, residues 166, 189, 285, and 571, as well as loops formed by residues 293−318 and 576−586, in the polymerase domain, and residues 1, 2, and 108 in the thioredoxin domain, were modeled by Dr. Suresh Singh (Merck Research Laboratories) using the Look homology modeling package from Molecular Applications Group. One missing Mg^{2+} ion in the exonuclease domain was modeled into the exonuclease active site based on the interactions with amino acid residues Asp5, Glu7, and Asp174, as suggested by the crystal structure (*51*). The primer−template DNA sequence was remodeled as the human *N-ras* mutational hotspot sequence shown in Figure 1B. Two 5′ terminal template nucleotides that were missing in the original crystal structure (*51*) were added in the canonical B-DNA conformation (*53*), using Insight II 97.0

A

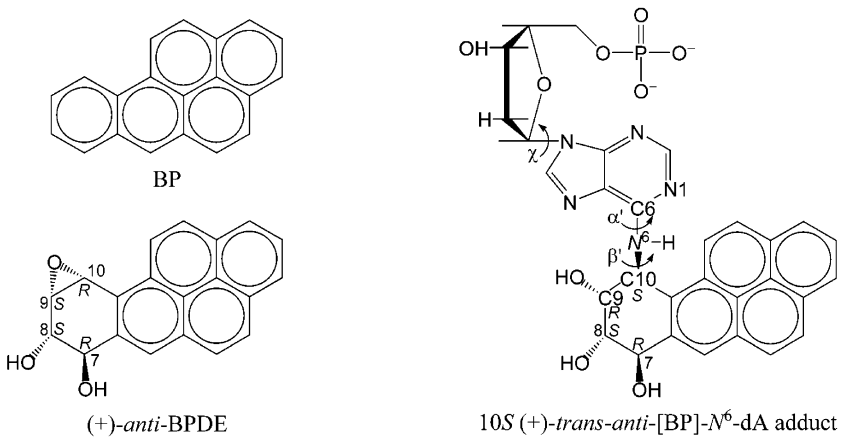

B

```
5'-pT1--pG2--pT3--pA4--pC5--pT6--pC7-pT8-pT9-pC10-pT11-3' dNTP
    |    |    |    |    |    |    |   |   |    |    |        |
3'-tA15-tC14-tA13-tT12-tG11-tA10-tG9-tA8-tA7-tG6--tA5----tA*4-tC3-tA2-tG1-5'
```

FIGURE 1: (A) Structures of BP, (+)-*anti*-BPDE, and 10*S* (+)-*trans*-*anti*-[BP]-*N*^{6}-dA adduct. Torsion angles α' and β' are defined as α', N1−C6−N6−C10(BP); β', C6−N6−C10(BP)−C9(BP). (B) Human *N*-*ras* codon 61 sequence employed in the MD simulations for the primer−template DNA. p and t denote the primer and template, respectively. tA*4 is the modified adenine residue on the template strand.

(Accelrys, Inc., a subsidiary of Pharmacopeia, Inc.). The incoming nucleotide was remodeled as dTTP, and hydroxyl groups were added to the 3′ termini of the primer and the incoming nucleotide, since dideoxynucleotides were present in the original crystal structure (*51*). To alleviate steric close contacts, a total of 50 steps of steepest descent minimization was carried out on the ternary complex with all the main chain atoms fixed, using the *Sander_classic* module in the AMBER 6.0 package (*54*). This minimized structure then served as the starting structure for the molecular dynamics simulation for the unmodified control.

To create the adduct structure, we docked a 10*S* (+)-*trans*-*anti*-[BP]-*N*^{6}-dA adduct, which was excised from an NMR solution structure in which a dG is opposite the modified dA (since no NMR solution structures for this adduct are available with a normal partner dT opposite the lesion) (*38*), to the template strand of the minimized unmodified T7 DNA polymerase ternary complex. Then we adjusted the carcinogen-base linkage torsion angles α' and β' (see Figure 1A) to position the BP moiety with minimal steric close contacts within the polymerase active site region. The only location in which the bulky carcinogen could fit without extensive disruption of protein−DNA interactions was in the open pocket on the major groove site of the template. In this modeling work, we were guided by the preferred χ, α', β' domains determined by previous work (*55*). Small adjustments in DNA backbone torsions adjacent to the modification site on the template strand were also required to achieve a starting structure with essentially no collisions. Both *anti* and *syn* glycosidic conformations of the adducted adenine were modeled. The incoming nucleotide was remodeled as dATP to create an A*−A mismatch in the polymerase active site. A total of 100 steps of steepest descent and 150 steps of conjugate gradient minimization with protein residues fixed was then applied. The minimized structures then served as the starting structures for molecular dynamics simulations. The torsion angles χ, α', β' were −127.6°, 170.3°, −114.9° (*anti* conformation) and 44.3°, 4.6°, −112.8° (*syn* conformation), respectively, in these structures. The structures with dTTP, dCTP, and dGTP opposite the modified templating adenine were remodeled from the *anti* tA*4 DNA−polymerase complex by replacing the dATP with the respective dNTPs (see Results and Discussion). Molecular modeling was carried out using Insight II 97.0 from Accelrys, Inc.

Force Field Parameters. We employed the partial charges for the 10*S* (+)-*trans*-*anti*-[BP]-*N*^{6}-dA adduct, which had been computed previously (*55*, *56*). To obtain the partial charges for dTTP and dATP, we remodeled the base of the incoming ddGTP from the T7 DNA polymerase ternary crystal structure (*51*) to A or T and added 3′-OH to the sugar, using Insight II 97.0. We then applied Hartree−Fock calculations with 6-31G* basis set to compute the electrostatic potential using Gaussian 94 (*57*), fitted to each atomic center with RESP (*58*), and normalized the charges to maintain a charge of −4 on the incoming nucleoside triphosphate. The same procedure was also employed for dCTP and dGTP. The partial charges for all four dNTPs are shown in Tables S1, S2, S3, and S4 of Supporting Information. Bond angle parameters added to the force field for the adducts, assigned by analogy to chemically similar atom types already available in the *parm98* parameter set (*59*), are the same as given previously (*56*).

Molecular Dynamics Simulation. Molecular dynamics simulations were carried out using the *Sander* module in the AMBER 6.0 package (*54*) with the *parm98* parameter set (*59*). The particle mesh Ewald (PME) method (*60*, *61*) was used to treat long-range electrostatic interactions. A 9-Å cutoff was applied to the nonbonded Lennard-Jones interactions. The SHAKE algorithm (*62*) was applied to constrain all bonds involving hydrogen atoms with a tolerance of 10^{-6} Å, and a 2-fs time step was used in the dynamics simulations. The translational motion of the center of mass was removed every 1 ps. Furthermore, visual inspection of the trajectories revealed no abnormal overall rotation of the protein−DNA complexes, indicating that energy leakage from internal motion to global rotation through the "flying ice cube effect" (*63*) is not contributing in this case.

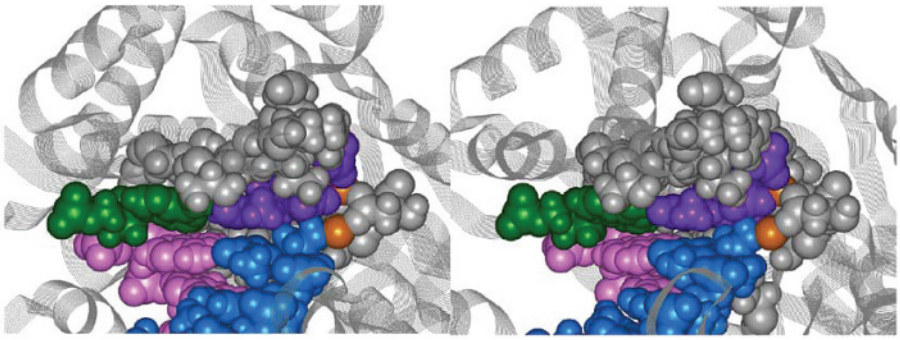

FIGURE 2: Stereoview of the active site region of the T7 DNA polymerase. The protein is in gray lines. The primer−template DNA, incoming dNTP, Mg^{2+} ions, and protein residues that are in close contact with DNA are in CPK. The color code is protein, gray; primer, blue; template, magenta; incoming dNTP, purple, template adenine, green; Mg^{2+}, orange. All stereo images are constructed for viewing with a stereoviewer.

A total of 1000 steps of steepest descent and 4000 steps of conjugate gradient minimization was first applied to the modeled loop residues with an $\epsilon = 4r$ distance-dependent dielectric function. This was followed by an additional total of 2000 steps of steepest descent and 8000 steps of conjugate gradient minimization with all main chain atoms fixed, also using an $\epsilon = 4r$ dielectric function. These minimizations were carried out using the *Sander_classic* module in AMBER 6.0. Then, 40 Na^+ ions were added to the system for neutralization using the *LEap* module in AMBER 6.0. After adding the 503 crystallographic water molecules, the system was solvated with a rectangular box of TIP3P water molecules (*64*) which extended ~9 Å from the polymerase−DNA ternary complex atoms in each direction. The number of water molecules in the rectangular box was minimized by optimizing the orientation of the box using the Simulaid program (*65*), which yielded a periodic box size of about 90 × 100 × 130 Å for the three polymerase−DNA complex systems. The number of water molecules (in addition to the 503 crystallographic water molecules) added to solvate the simulated systems are as follows: unmodified control, 27 330; *anti* tA*4 structure, 27 643; *syn* tA*4 structure, 27 125; A*−dTTP structure, 27 743; A*−dCTP structure, 27 677; A*−dGTP structure, 27 797. The total number of atoms in the system including water molecules and counterions was then 97 104, 98 080, 96 526, 98 380, 98 180, and 98 543 for the unmodified control, *anti* tA*4 structure, *syn* tA*4 structure, A*−dTTP structure, A*−dCTP structure, A*−dGTP structure, respectively.

All systems followed the same minimization and equilibration protocols. First, the water molecules and counterions were minimized for 5000 steps of steepest descent with solute atoms fixed, followed by 20-ps initial dynamics at 10 K with 1.0 kcal/mol restraints on the solute to allow the solvent to relax. The whole system was then heated from 10 to 300 K over 50 ps using the Berendsen coupling algorithm (*66*) with a coupling parameter of 1.0 ps, followed by 50-ps dynamics with 1.0 kcal/mol restraints on the solute. Finally, the whole system was further equilibrated by 50-ps dynamics without restraints. Production simulation was then continued at atmospheric pressure with a 1.0-ps coupling parameter and 300 K for 1.0 ns.

RESULTS AND DISCUSSION

In this work, we have carried out molecular modeling and molecular dynamics simulations of a polymerase primer−template ternary complex with the template DNA containing a 10*S* (+)-*trans*-*anti*-[BP]-N^6-dA adduct positioned within the active site of the T7 DNA polymerase. We investigated the effects of each of the four possible incoming dNTPs opposite the lesion on the size and shape of the binding pocket. The unmodified adenine residue was also investigated as a control.

The BP Residue Is Positioned in an Open Pocket of the T7 DNA Polymerase on the Major Groove Side of the Templating Modified Adenine. Our modeling studies began with an effort to locate a position within the T7 DNA polymerase where the bulky BP ring system (Figure 1) can be placed without disrupting the intrinsic structures and interactions of amino acid residues in the polymerase. Both experimental (*37*, *38*) and computational (*56*) results indicate that the BP moiety in the 10*S* (+)-*trans*-*anti*-[BP]-N^6-dA adduct is positioned stacked on the 3′-side of the modified adenine. An examination of the active site of T7 DNA polymerase containing this 10*S* adduct reveals however that there is no room in the polymerase active site region to accommodate the bulky BP on the 3′-side of the modified adenine without significantly distorting the polymerase structure (Figure 2). We suggest (see below) that such a conformation would stall, or block the polymerase at that site. However, the T7 DNA polymerase ternary complex contains an open pocket on the major groove side of the templating base which can accommodate a bulky moiety such as the BP residue. In such a structure, the BP residue is positioned on the major groove edge of the adenine base; since the N^6 adenine position is on the base major groove edge, glycosidic torsion angle values in both the *anti* and the *syn* domain place the BP ring system on the major groove side. We thus created starting models with an incoming dATP with minimal steric crowding for both types of glycosidic angle orientations. These modeling studies were guided by employing the energetically preferred domains for the χ, α', and β' torsion angles (see Figure 1) that were computed previously (*55*). The starting models were then subject to 1 ns of molecular dynamics, following a 170-ps equilibration period. A control simulation using an unmodified template was also carried out. Figure S1 in Supporting Information provides data on the stabilities of these simulations, showing reasonably stable fluctuations after ~400 ps. Figure S2 shows the time dependence of the χ, α', and β' linkage torsion angles (Figure 1), and these also indicate the

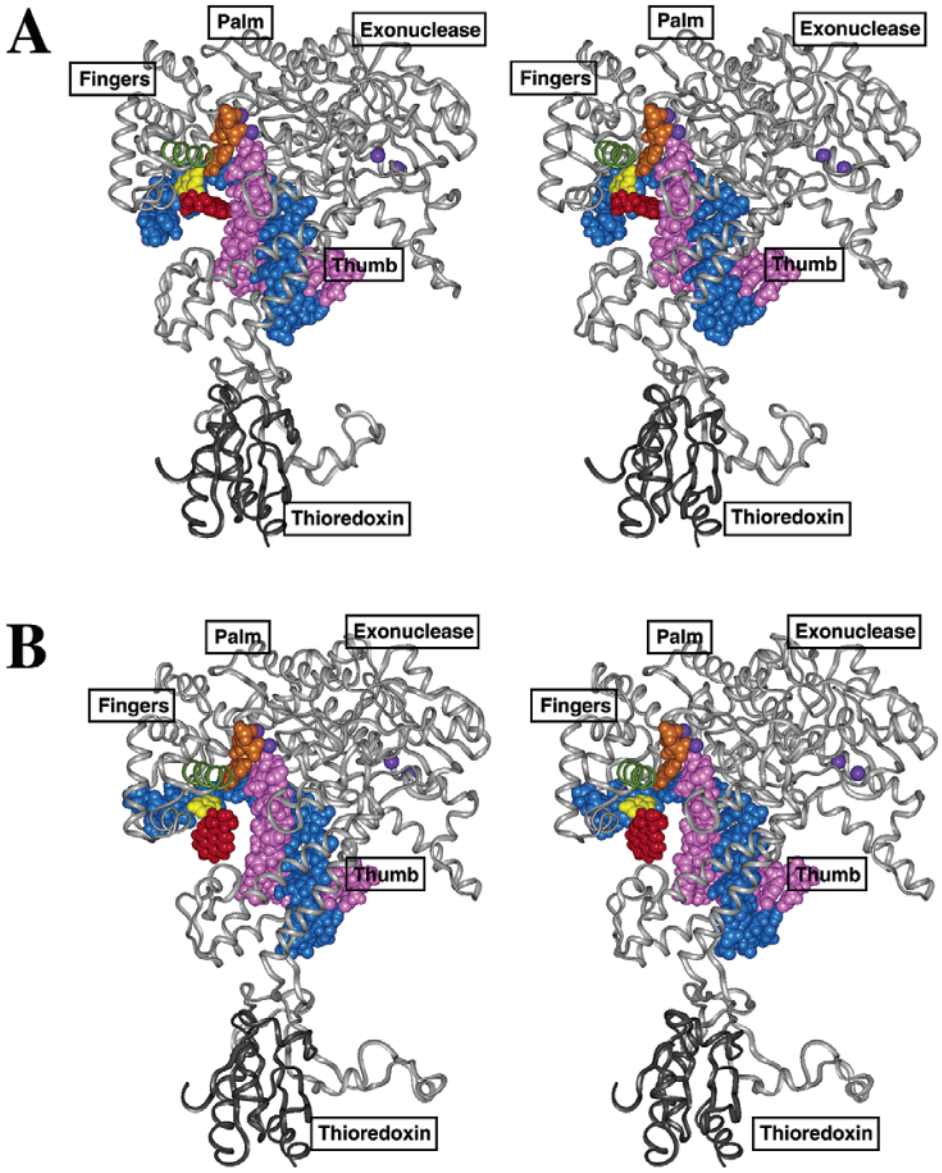

FIGURE 3: Stereoviews of the simulated protein complex containing thioredoxin and T7 DNA polymerase ternary structure with modified adenine and incoming dATP after 1-ns MD simulation. The glycosidic conformation of the modified adenine tA*4 is (A) *anti* or (B) *syn*. The thioredoxin is in dark gray ribbon. The polymerase is in light gray ribbon with the thumb, palm, fingers, and exonuclease domains denoted, and the O helix is in light green ribbon. The DNA residues and Mg^{2+} ions are shown in CPK. The color code is magenta, primer; blue, template; yellow, modified adenine base of tA*4; red, BP; orange, incoming dATP; purple, Mg^{2+} ions.

stable positioning of the templating adenine base and its linked BP moiety.

Figure 3 shows structures of the T7 DNA polymerase ternary complex with the modified adenine in the *anti* or *syn* glycosidic bond conformation and with dATP opposite the adduct at the end of a 1-ns simulation. The modified adenine residue, particularly its BP ring system, is positioned very differently in the *anti* and *syn* conformations. As shown in Figure 3A, in the case of the *anti* conformation, the BP residue has substantial van der Waals interactions with both primer−template DNA and protein residues, which tend to shield the BP residue from interactions with solvent molecules. However, in the case of the *syn* conformation, the BP has much less contact with protein residues, virtually no interactions with DNA, and is exposed to the solvent environment (Figure 3B). This difference is clearly evident from a study of the solvent-accessible surface area of the aromatic part of the BP residue. We computed solvent-accessible surface areas of 178 Å^2 for the *anti* conformation and 212 Å^2 for the *syn* case, using the Connolly algorithm (with probe radius 1.4 Å) implemented in Insight II 97.0 (*67*).

The BP-Modified Adenine Is Displaced Away from the Polymerase Active Site to Avoid Collisions between BP and the Primer−Template DNA Residues. In the control unmodified template case the templating tA4 adenine base (Figure 1) is in extensive contact with a protein pocket comprised of polymerase residues, Thr523, Tyr526, Gly527, and Tyr530, within the active site of the polymerase. As shown in Figure 4A, the adenine base is well shielded from the solvent by a "wall" comprised of these residues. However, in the case of the modified adenine tA*4 with dATP, the modified adenine base is displaced out of this pocket region in both the *anti* and *syn* structures (Figure 4B,C). To further assess the displacement of this modified adenine residue, we monitored the distance between Cα of Gly527 and N7 of

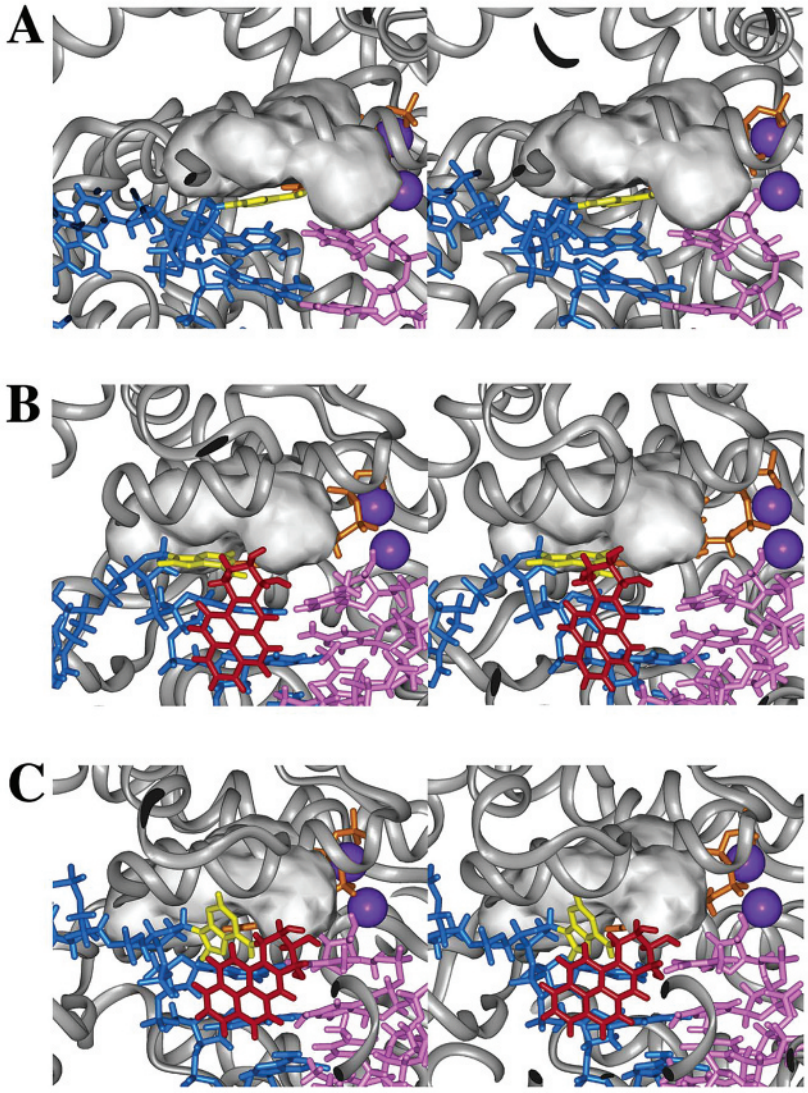

FIGURE 4: Stereoviews of the active site regions for the simulated T7 DNA polymerase complexes. (A) Unmodified control. (B) Modified tA*4 *anti* structure. (C) Modified tA*4 *syn* structure. The polymerase is in gray ribbon, and the gray protein pocket is comprised of Thr523, Tyr526, Gly527, and Tyr530. The DNA residues are in stick, and the Mg^{2+} ions are in CPK. The color code is magenta, primer; blue, template; yellow, modified adenine base of tA*4; red, BP; orange, incoming dNTP (dTTP in A, dATP in B and C); purple, Mg^{2+} ions.

tA*4, since the interaction between this highly conserved glycine residue (Gly527) and the template base is crucial for positioning of the template as observed in the crystal structure (*51*). The time dependence of the Cα−N7 distance between Gly527 and tA*4 is shown in Figure S3 (Supporting Information). The average Cα−N7 distance is 3.6 ± 0.4 Å in the unmodified control, while it is 5.6 ± 0.4 and 5.7 ± 0.3 Å in the *anti* and *syn* tA*4−dATP mismatch structures, respectively, over the 0.5−1 ns time frame. Clearly, the template base tA*4 is displaced away from the optimal position for maintaining the conserved interaction with the glycine residue, Gly527, in both cases. This also effectively increases the distance between the template residue tA*4 and the incoming dATP, as demonstrated by increased C1′−C1′ distance between these two residues in the A*−A mismatch structures (Figure S4). The average C1′−C1′ distance is 11.0 ± 0.3, 11.9 ± 0.2, and 11.8 ± 0.2 Å in the unmodified control tA4−dATP, and *anti* and *syn* tA*4−dATP mismatch structures, respectively, over the 0.5−1 ns time frame.

As shown in Figure 4B the modified adenine base in the *anti* tA*4−dATP mismatch structure is clearly shifted from the polymerase active site. The origin of this displacement is the presence of the bulky BP ring system. Were the adenine to remain in its normal position, the BP residue would collide with adjacent primer and template residues (tA5, tG6, tA7, pT8, and pT9), which are tightly held within the polymerase DNA binding tract (Figure 5A). However, by repositioning tA*4 the BP ring system is properly positioned to be favorably in contact with these same residues through van der Waals interactions. Indeed, the computed trajectory-averaged van der Waals interaction energies between BP and the primer−template DNA over the 0.5−1 ns time frame are favorable (tA5, −2.0 kcal/mol; tG6, −1.0 kcal/mol; tA7, −0.9 kcal/mol; pT8, −1.5 kcal/mol; pT9, −1.2 kcal/mol).

This structure is also partly stabilized by hydrogen bonding interactions between the BP residue and two polymerase amino acids. Specifically, the O9−HO9 hydroxyl group on the benzylic ring is involved in a bifurcated hydrogen bond with Lys536 and Gln539 (Figure 5B). The time dependence of the hydrogen bond distances and angles for this bifurcated hydrogen bond, specifically the amino group of Lys536 (donor) to O9 (acceptor) and O9−HO9 (donor) to OE1 of Gln539 (acceptor), shown in Figure S5, reveals occupancies of ∼28 and ∼16%, respectively, in the last 500 ps of the

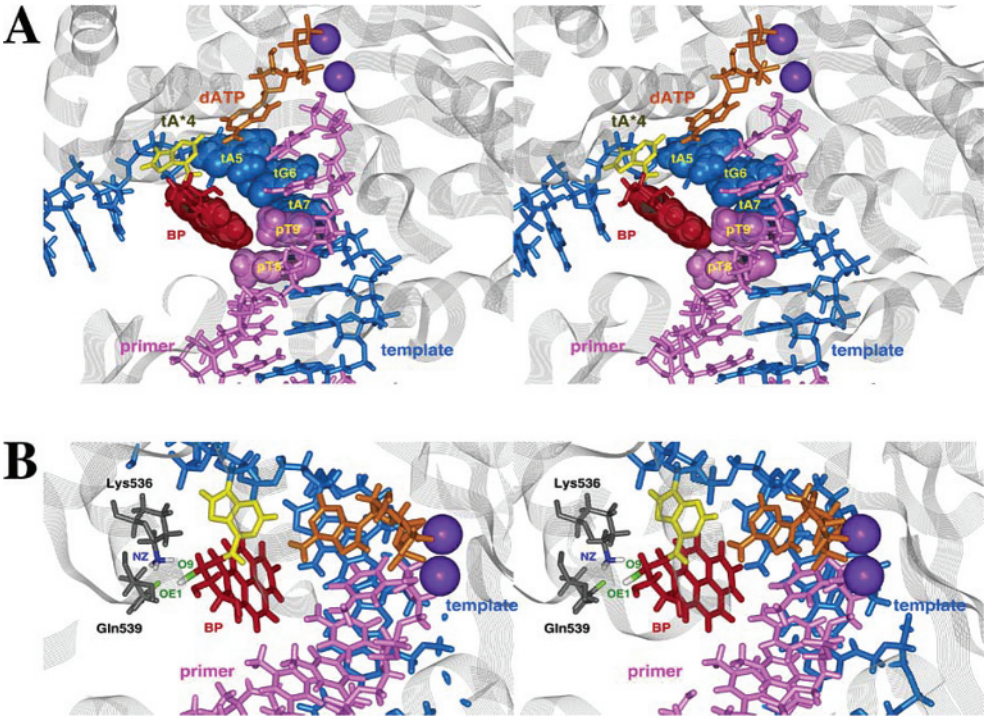

FIGURE 5: Stereoviews of the T7 DNA polymerase complex with the modified adenine tA*4 *anti*, showing (A) steric hindrance between BP and primer−template DNA and (B) hydrogen bonds between BP and protein residues, Lys536 and Gln539. The protein is in gray lines. The BP and the DNA residues (tA5, tG6, tA7, pT8, and pT9) involved in the steric interactions are in CPK in A. Other DNA residues in A are in stick. All DNA residues and amino acids, Lys536 and Gln539, in B are in stick. The Mg^{2+} ions are in CPK. The color code is magenta, primer; blue, template; yellow, modified adenine base of tA*4; red, BP; orange, dATP; purple, Mg^{2+} ions; gray, Lys536 and Gln539 in B. The atoms involved in the hydrogen bond interactions in B are colored by atom: nitrogen, blue; oxygen, green; hydrogen, white.

simulation. During the remainder of the simulations, distances are not within the hydrogen bonding range, but are close enough to afford some stabilization through favorable electrostatic interactions. These hydrogen bonding, or favorable electrostatic interactions, aid in maintaining the displaced position of the template adenine base tA*4 in the active site.

As shown in Figure 4C, when the modified template tA*4 is *syn*, the adenine residue of tA*4 is totally displaced out of the pocket comprised of Thr523, Tyr526, Gly527, and Try530; this is in contrast to the unmodified template structure, where the adenine of tA*4 is fully shielded in this pocket (Figure 4A). In fact, the *syn* tA*4 base residue is nearly perpendicular to the normal primer−template DNA base pair plane, and is significantly displaced from the active site of the polymerase. Moreover, due to the *S* absolute configuration at the linkage site and the *syn* glycosidic conformation of the modified base of tA*4, the bulky BP moiety has no close contacts with the primer−template DNA, but instead is significantly exposed to the solvent.

The Incoming dATP Is Well Accommodated within the Active Site of the T7 DNA Polymerase Opposite the Anti BP-Modified Adenine Base. (1) The Hydrophilic Sugar Triphosphate Portion of the Incoming dATP Has Stabilizing Interactions with Amino Acid Residues of the T7 DNA Polymerase. We found that the hydrophilic sugar triphosphate of the dTTP in the unmodified control structure is involved in extensive nonspecific interactions with protein residues Lys522, Arg518, Tyr526, His506, Gly478, Glu480, Leu479, as well as with the conserved Asp475 and Asp654 residues that are chelated with both of the Mg^{2+} ions (Figure 6A). These interactions are also present in the crystal structure of the T7 DNA polymerase ternary complex (*51*). Furthermore, these nonspecific interactions between polymerase residues and the sugar triphosphate of the incoming nucleotide are mostly preserved in the structure with the incoming dATP opposite the modified template adenine base of tA*4 (Figure 6B,C). As shown in Table 1, hydrogen bond analysis of the interactions between these amino acid residues and the sugar triphosphate portion of the dNTP reveal that the important hydrogen bond interactions between the hydrophilic sugar triphosphate of the complementary dTTP and the polymerase in the unmodified ternary complex are largely preserved in the tA*4−dATP mismatch structure, irrespective of whether the modified tA*4 is *anti* or *syn*.

(2) The Hydrophobic Base Portion of the Incoming dATP Is Well Encased in the Hydrophobic dNTP Base Binding Pocket of the T7 DNA Polymerase when the BP-Modified Template Adenine Is Anti. Geometric selection employed by DNA polymerases is believed to play a determining role in dictating the fidelity and efficiency of DNA replication (*7*, *19*, *68*−*72*). The size and shape of the active site hydrophobic binding pocket for the base moieties of the incoming dNTP are crucial for selecting the right nucleotide (*7*, *71*). As shown in Figure 7A, the dNTP base binding pocket in the unmodified structure, comprised of pT11, tA5 (floor), Tyr526, Gly527 (ceiling), Gln615, Arg429, Glu480, Tyr530, Asn611 (back wall which is against the minor groove), Thr523 (front wall which is against the major groove), and tA4 (far wall which is the template base) (*72*), accommodates the hydrophobic base portion of the incoming dTTP with the right shape and size (Figure 8A), as expected.

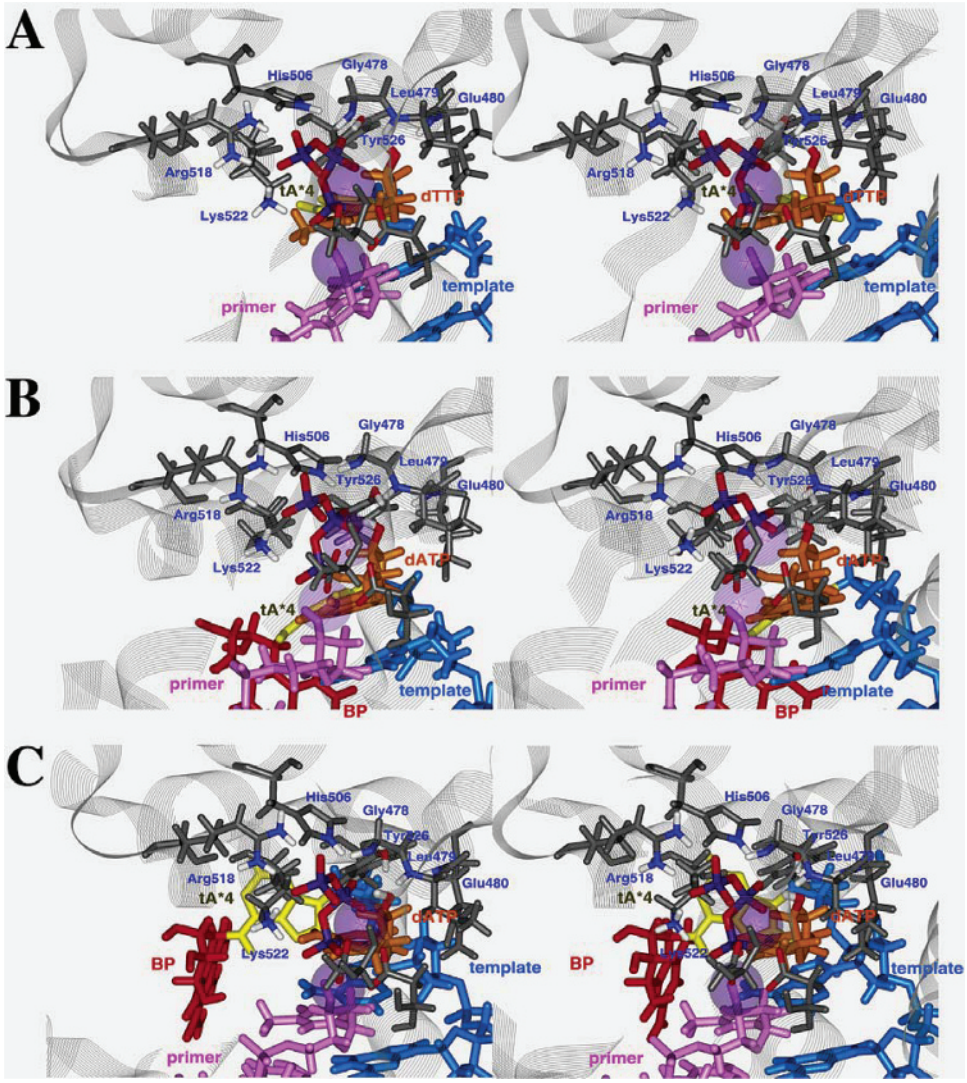

FIGURE 6: Stereoviews of the active sites of the simulated T7 DNA polymerase complexes. (A) Unmodified control. (B) Modified tA*4 *anti* structure. (C) Modified tA*4 *syn* structure. The protein is in gray lines. The DNA residues and the amino acid residues (Lys522, Arg518, Tyr526, His506, Gly478, Glu480, Leu479) involved in the hydrogen bond interactions with dNTP (dTTP in A, dATP in B and C) as well as Asp475 and Asp654 are in stick. The Mg^{2+} ions are in purple transparent spheres. The color code is primer, magenta; template, blue; dNTP, orange; modified templating base, yellow; BP, red; amino acids involved in the hydrogen bond interactions as well as Asp475 and Asp654, dark gray. The atoms involved in the hydrogen bond and electrostatic interactions are colored by atom: nitrogen, blue; oxygen, red; phosphorus, purple, hydrogen, white.

However, in the BP-modified ternary complex structures, the hydrophobic base portion of the mismatched dATP has substantially different interactions with the polymerase and primer−template DNA when the BP-modified template base tA*4 is *anti* or *syn*. As shown in Figures 4B and 7B, the far wall of the dNTP base binding pocket (tA*4) is displaced away from the catalytic active site, when the modified template base tA*4 is *anti*, due to steric hindrance caused by the BP residue; this effectively enlarges the size and changes the shape of the binding pocket for the incoming dNTP. As shown in Figure 8B, this expanded binding pocket has the proper size and geometric complementarity for a mismatched adenine residue, and therefore accommodates the mismatched incoming dATP quite well. An A−A orientation similar to our tA*4−dATP mismatch structure in the polymerase active site has been experimentally observed in a crystal structure containing this type of mismatch (NDB ID: RR0033, A1912−A1927) (*73*). On the other hand, in the case of the *syn* tA*4 structure, the template adenine base is nearly perpendicular to the normal primer−template DNA base pair; this causes disruption of the dNTP binding pocket (Figure 7C), which would make accommodation of an incoming dATP implausible.

The Primer 3′-Hydroxyl Is in Position to Readily Attack the α-Phosphate of the Incoming dATP in Modified and Unmodified Template−Primer Polymerase Complexes. A two-metal phosphoryl transfer mechanism involving nucleophilic attack of the primer 3′-hydroxyl group on the α-phosphate of the incoming dNTP is employed by DNA polymerases to catalyze DNA replication (*10*, *51*, *74*, *75*). We monitored the distance between O3′ of the primer termini pT11 and Pα of the dTTP or dATP over the course of the simulation for both the unmodified control template and the tA*4−dATP mismatch structures (Figure S6). The trajectory average distance is 3.1 ± 0.1, 3.0 ± 0.1, and 3.0 ± 0.1 Å for the control, *anti* tA*4, and *syn* tA*4 structures, respectively, over the 0.5−1 ns time frame. This ∼3 Å distance brings the primer 3′-hydroxyl and the dATP α-phosphate within the range needed for successful nucleotidyl transfer.

Table 1: Hydrogen Bond Analysis of the Interactions between the Amino Acid Residues and the Sugar Triphosphate of the Incoming dNTP[a]

donor	acceptor	control (%)	tA*4 *anti* (%)	tA*4 *syn* (%)
Lys522 $N^{\zeta}-H^{\zeta 2}$	dNTP $O^{\alpha 1}$	91	69	64
Lys522 $N^{\zeta}-H^{\zeta 3}$	dNTP $O^{\alpha 1}$	5	22	15
Lys522 $N^{\zeta}-H^{\zeta 3}$	dNTP $O^{\gamma 3}$	95	69	64
Lys522 $N^{\zeta}-H^{\zeta 1}$	dNTP $O^{\gamma 3}$	5	22	15
Arg518 $N^{\eta 1}-H^{\eta 12}$	dNTP $O^{\gamma 3}$	100	100	100
Arg518 $N^{\eta 2}-H^{\eta 22}$	dNTP $O^{\gamma 2}$	100	100	100
His506 $N^{\epsilon 2}-H^{\epsilon 2}$	dNTP $O^{\beta 1}$	99	99	99
His506 $N^{\epsilon 2}-H^{\epsilon 2}$	dNTP $O^{\beta 3}$	23	16	21
Tyr526 $O^{\eta}-H^{\eta}$	dNTP $O^{\beta 1}$	100	21	7
Tyr526 $O^{\eta}-H^{\eta}$	dNTP O3′	1	86	96
dNTP O3′−H3′	Tyr526 O^{η}	47	3	1
Gly478 N−H	dNTP $O^{\gamma 2}$	47	98	81
Gly478 N−H	dNTP $O^{\beta 3}$	94	86	91
Glu480 N−H	dNTP O3′	99	96	93
Leu479 N−H	dNTP $O^{\beta 2}$	25	30	27

[a] The % occupancies were computed using the MOIL-View program (*84*) for each of the last 500-ps simulations.

Table 2: van der Waals Interaction Energies between BP and the Primer−Template DNA Residues[a]

	A*−dATP	A*−dTTP	A*−dCTP	A*−dGTP
tG1	0.0	0.0	0.0	0.0
tA2	0.0	0.0	0.0	0.0
tC3	−0.1	0.0	0.0	0.0
tA5	−2.0	−0.6	−1.2	−0.5
tG6	−1.0	−0.3	−0.3	−0.2
tA7	−0.9	−0.3	−0.2	−0.2
tA8	−0.2	−0.1	−0.1	−0.1
tG9	−0.1	0.0	−0.1	−0.1
tA10	0.0	0.0	0.0	0.0
tG11	0.0	0.0	0.0	0.0
tT12	0.0	0.0	0.0	0.0
tA13	0.0	0.0	0.0	0.0
tC14	0.0	0.0	0.0	0.0
tA15	0.0	0.0	0.0	0.0
pT1	0.0	0.0	0.0	0.0
pG2	0.0	0.0	0.0	0.0
pT3	0.0	0.0	0.0	0.0
pA4	0.0	0.0	0.0	0.0
pC5	0.0	0.0	0.0	0.0
pT6	−0.1	−0.1	−0.2	−0.3
pC7	−0.5	−0.3	−0.9	−2.1
pT8	−1.5	−1.3	−1.4	−1.9
pT9	−1.2	−1.5	−0.9	−0.4
pC10	−0.5	−0.4	−0.3	−0.1
pT11	−0.2	−0.2	−0.2	−0.1

[a] All energies are in kcal/mol. The modified template adenine tA*4 is *anti* in all cases.

dTTP, dCTP, and dGTP Are Poorly Accommodated in the Active Site Opposite the BP-Modified Adenine Base. Nucleotide incorporation experiments for the 10*S* (+)-*trans-anti*-[BP]-N^6-dA adduct on the template strand reveal that dATP is the base that is preferentially incorporated opposite the modified adenine by Sequenase 2.0, an *exo*$^-$ version of the T7 DNA polymerase, followed by smaller levels of dGTP and dTTP incorporation (*47*). We analyzed the structures of our simulated polymerase complexes to help rationalize these experimental findings on a molecular level.

(1) Displacement of the Adenine Residue Is Observed in all Four Cases of Incoming dNTPs Because of the Bulky BP Moiety. As shown above, the presence of the covalently linked bulky BP residue causes a displacement of the template adenine base within the polymerase active site in the tA*4−dATP complex (Figure 4). This, in turn, significantly changes the dimensions and geometries of the dNTP base binding pocket. To investigate the fit of the other dNTPs into the binding pockets, we carried out additional dynamics simulations with dTTP, dCTP, or dGTP with the structurally preferred *anti* glycosidic conformation of the BP-modified adenine residue. We found that all three structures, containing tA*4−dTTP, tA*4−dCTP, and tA*4−dGTP, respectively, are characterized by a displacement of the modified template adenine (Figure S7), as demonstrated by increased Cα−N7 distance between the conserved Gly527 residue and the modified tA*4. Specifically, the Cα−N7 distance between Gly527 and the tA*4 adenine is 5.4 ± 0.4, 5.5 ± 0.4, and 6.5 ± 0.2 Å in the tA*4−dTTP, tA*4−dCTP, and tA*4−dGTP structures, respectively, as compared to 3.6 ± 0.4 Å in the modified control, over the 0.5−1 ns time frame (Figure S8). We also superimposed the protein and DNA residues within the active site (i.e., Tyr526, Gly527, pT11, tA5, Thr523, Gln615, Arg429, Glu480, Tyr530, Asn611, Lys522, Arg518, His506, Gly478, Leu479, Asp475, and Asp654) of the modified tA*4−dNTP structures against the unmodified control, and found a substantial movement of the adducted adenine, while the other active site residues remain quite stable with RMSD of ∼1 Å in all cases. The nature of the displacement of the adducted template adenine is somewhat influenced by the different incoming dNTPs, as shown in Figures 9 and S9. This is manifested by the differential positioning of the covalently bound BP, as it contacts the primer−template DNA at distinctive sites in the structures containing different dNTPs (Figure S9). Specifically, the BP hydrophobic ring system has van der Waals contacts with pT8 and pT9 residues on the primer strand in the A*−dTTP structure, while it contacts with pC7 and pT8 in the tA*4−dGTP structure. In the tA*4−dCTP structure, the BP residue however contacts with tA5, pC7, pT8, and pT9 on both primer and template strands. We recall that in the tA*4−dATP structure the BP residue has van der Waals contacts with tA5, tG6, tA7, pT8, and pT9 on the primer−template DNA strands; thus, the positioning of BP and its covalently linked adenine residue is clearly influenced by the incoming dNTP. Our computed van der Waals interaction energies between BP and the primer−template DNA residues (Table 2) are in line with these observations.

(2) The Small-Sized Pyrimidine Bases dTTP and dCTP Are Poorly Held in the Enlarged and Distorted dNTP Base Binding Pockets. Since the modified adenine (far wall of the dNTP base binding pocket) is displaced away from the active site region, an enlarged dNTP base binding pocket is created; this causes an inadequate steric fit of the smaller dTTP and dCTP, which no longer sufficiently occupy all of the available space in this expanded pocket. In the tA*4−dTTP structure, the base of the incoming dTTP flips into a conformation that is perpendicular to the primer−template DNA base pair plane and the template adenine; this significantly distorts the 3′-terminal base pair (floor of the dNTP base binding pocket) as demonstrated by the severe buckle (Figure 9A). Furthermore, it also helps to create a substantially deformed dNTP base binding pocket, which poorly accommodates the incoming dTTP (Figure 9A). As shown in Figure 9B, in the tA*4−dCTP structure, the nascent base pair is severely distorted with the cytosine base plane

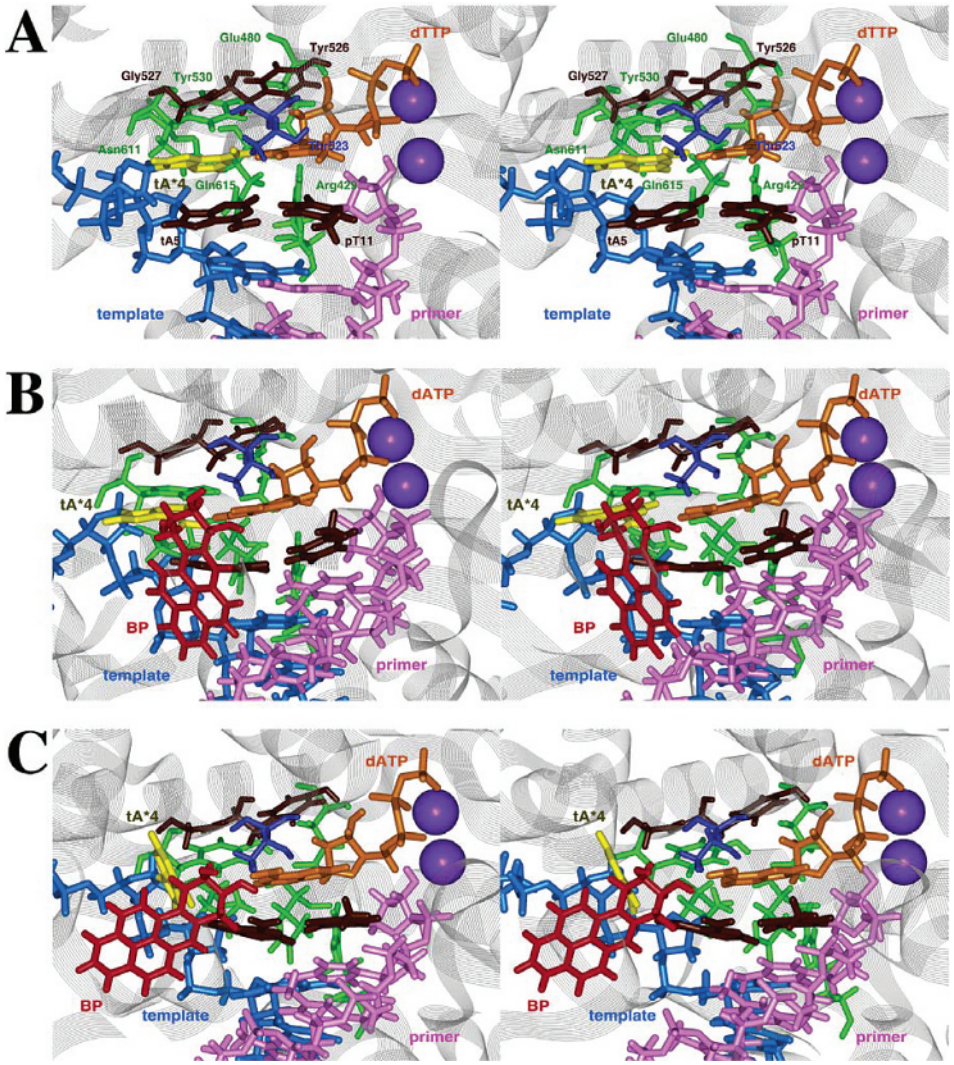

FIGURE 7: Stereoviews of the dNTP base binding pockets of the simulated T7 DNA polymerase complexes. (A) Unmodified control. (B) Modified tA*4 *anti* structure. (C) Modified tA*4 *syn* structure. The protein is in gray lines. The DNA and amino acid residues defining the dNTP base binding pocket are in stick. The Mg^{2+} ions are in CPK. The color code is magenta, primer; blue, template; orange, dNTP; brown, ceiling (Tyr526 and Gly527) and floor (pT11 and tA5 bases); dark blue, front wall (Thr523); green, back wall (Gln615, Arg429, Glu480, Tyr530, and Asn611); yellow, far wall (tA4 base in A and tA*4 base in B and C).

almost perpendicular to the template adenine; in this respect, it is similar to the tA*4−dTTP structure with inadequate steric fit of the small cytosine base. While the cytosine is similar in size to thymine, it lacks the methyl group; this further weakens the already diminished van der Waals interactions with the hydrophobic nucleotide base binding pocket. The incoming dCTP appears to have even less van der Waals contacts with the hydrophobic dNTP base binding pocket in the tA*4−dCTP structure than in the tA*4−dTTP case (Figure 9). This correlates with the experimental finding that dCTP is virtually not incorporated opposite the lesion by T7 DNA polymerase (*47*).

*(3) The Incoming dGTP Is Misaligned with the Adducted Template Adenine Base in tA*4, Causing Unfavorable Accommodation within the dNTP Base Binding Pocket.* The size of the dNTP base binding pocket is enlarged by the displacement of the BPDE-adducted template, irrespective of which dNTP is the incoming nucleotide; this enlarged pocket would appear to be suitable for the larger guanine base. However, if dGTP is inserted, the modified adenine base becomes even further displaced, producing a dNTP base binding pocket that no longer closely fits the shape of the guanine base. The position of the incoming dGTP is rather inflexible because of the strong electrostatic interactions between the polymerase (together with the Mg^{2+} ions) and the highly charged sugar triphosphate portion of the dNTP, as well as the steric constraints of the "closed" polymerase conformation. With this anchoring of the dGTP, as shown in Figure 10A, H1(N1) of dGTP would crowd H2(C2) of the modified adenine, if the tA*4−dGTP pair were to assume the same relative positions as the tA*4−dATP pair. To alleviate this crowding and electrostatic repulsion, the modified template adenine is shifted away (Figure 10B), which leaves a dNTP base binding pocket that is no longer able to snugly accommodate the incoming dGTP. Thus, the A and G Watson−Crick edges are completely misaligned as compared to an observed A−G mismatch crystal structure (Figure 10C) (*73*).

In summary, without BP modification, dTTP is the preferred ligand for the polymerase−primer−template complex with a templating adenine; however, with a BP modification to the adenine residue on the template strand, our simulations suggest that the preferred ligand for such a polymerase−DNA complex is dATP due to geometric

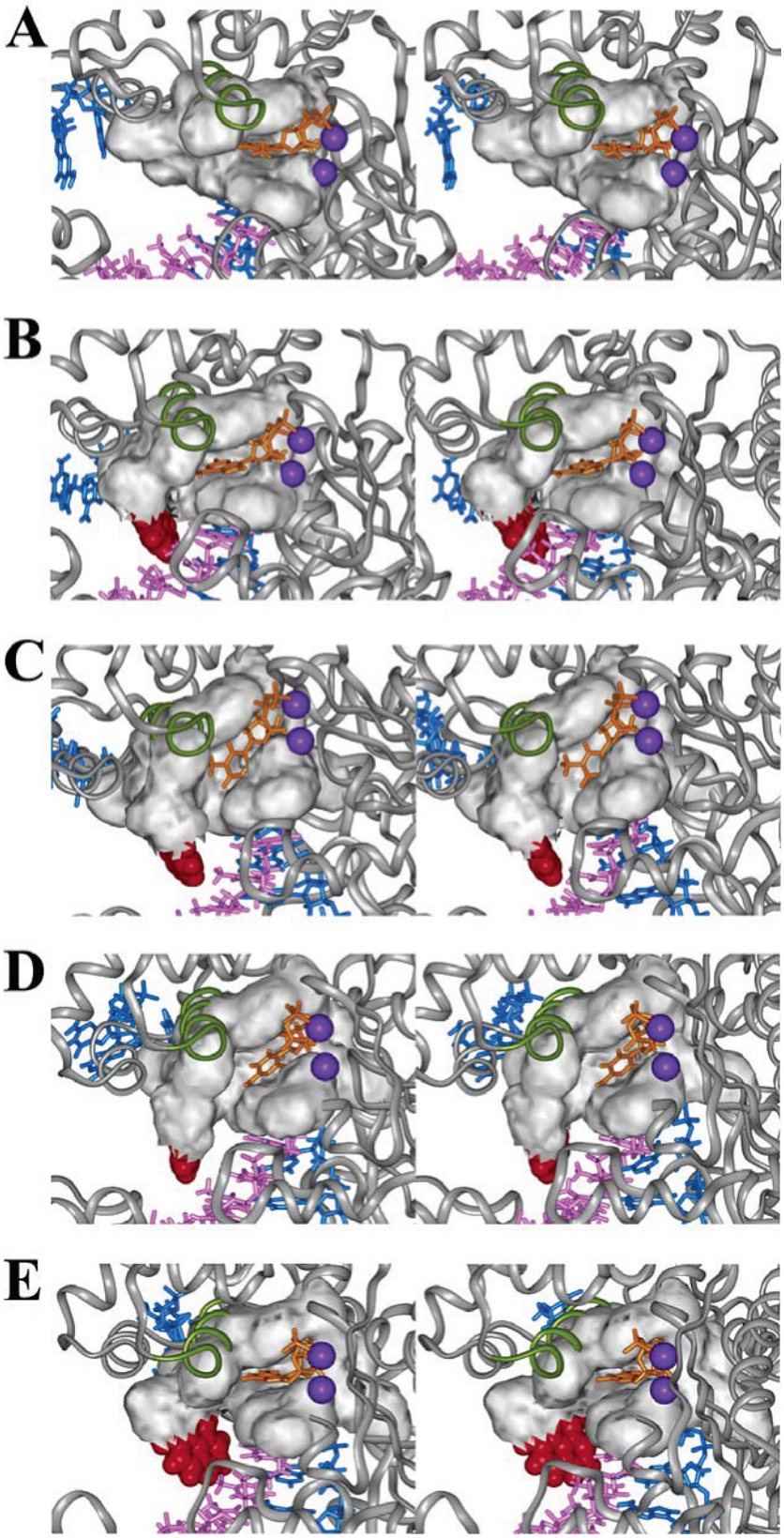

FIGURE 8: Stereoviews of the dNTP base binding pockets with the inserted dNTPs. (A) Unmodified control with tA4−dTTP in the polymerase active site. (B) Simulated tA*4−dATP (tA*4 is *anti*), (C) tA*4−dTTP, (D) tA*4−dCTP, and (E) tA*4−dGTP structures. The protein is in gray ribbon with the O helix in light green. The DNA residues are in stick. The Mg^{2+} ions are in CPK. The dNTP base binding pockets (comprised of pT11, tA5, Tyr526, Gly527, Gln615, Arg429, Glu480, Tyr530, Asn611, Thr523, and tA4/tA*4) are in gray. The color code is magenta, primer; blue, template; purple, Mg^{2+} ions; orange, dNTP.

changes in the dNTP base binding pocket (Figure 8). Taken together with our simulated structures for the incoming dTTP, dCTP, and dGTP, our studies show that the altered dNTP base binding pocket within the polymerase−DNA complex cannot accommodate these other incoming dNTPs as favorably as dATP. In the case of the unmodified template

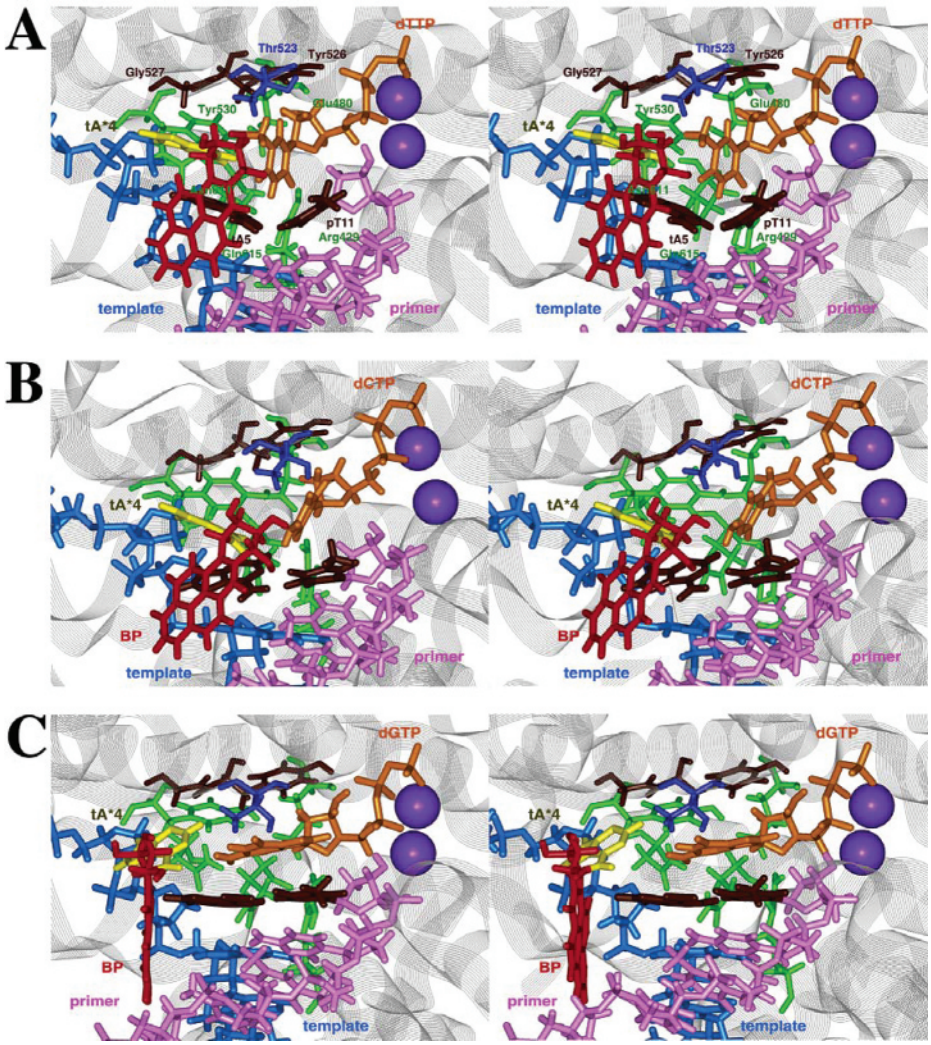

FIGURE 9: Stereoviews of the dNTP base binding pockets of the simulated T7 DNA polymerase with incoming dTTP, dCTP, and dGTP. (A) tA*4−dTTP structure. (B) tA*4−dCTP structure. (C) tA*4−dGTP structure. The protein is in gray lines. The DNA and amino acid residues defining the dNTP base binding pocket are in stick. The Mg^{2+} ions are in CPK. The color code is magenta, primer; blue, template; orange, dNTP; brown, ceiling (Tyr526 and Gly527) and floor (pT11 and tA5 bases); dark blue, front wall (Thr523); green, back wall (Gln615, Arg429, Glu480, Tyr530, and Asn611); yellow, far wall (tA*4 base).

adenine, kinetic measurements revealed that the catalytic efficiency for insertion of dATP opposite A is 91 M^{-1} s^{-1} (*76*) compared to 16 μM^{-1} s^{-1} for the normal partner (*77*). Specific data for dNTP incorporation efficiency do not, to our knowledge, appear available for adenine modified by the 10*S* (+)-*trans*-*anti*-[BP]-N^6-dA adduct; however, our modeling suggests that the catalytic efficiency for insertion of dATP as well as the other mismatched incomers should be poor compared to the unmodified template, since in all cases an altered dNTP binding pocket is produced by the bulky adduct.

Structural Explanations for Differences in T7 DNA Polymerase Stalling Patterns Observed with Stereoisomeric 10S and 10R Lesions. Primer extension experiments showed that the 10*S* (+)-*trans*-*anti*-[BP]-N^6-dA adduct predominantly blocks the T7 DNA polymerase when positioned on the template strand (*47*). These studies showed that in the case of the 10*S* (+)-*trans*-*anti*-[BP]-N^6-dA adduct, the polymerase stalls one base 3′ to the lesion as well as opposite the lesion after successful incorporation of a dNTP opposite the 3′-flanking base. However, in the case of the stereoisomeric 10*R* (−)-*trans*-*anti*-[BP]-N^6-dA adduct, the polymerase primarily stalls opposite the lesion (*47*). We sought to delineate possible structural explanations for these observed differences in the stalling patterns.

When covalently linked to adenine residues, BP is predominantly intercalated between the base pairs of the DNA double helix in NMR solution structures (*36*−*42*). The BP tends to be positioned stacked on the 3′-side of the modified adenine in the 10*S* (+)-*trans*-*anti*-[BP]-N^6-dA adduct (*37*, *38*, *40*), while it is stacked on the 5′-side in the 10*R* (−) case (*36*, *39*), and these are energetically favored domains (*55*). In the context of a replicative DNA polymerase such as T7, we suggest that the preferred orientations at the chiral C10 carbon atom of the BP residue may be maintained at or near the single strand−double strand primer−template complexes. This hypothesis is consistent with a stalling of the polymerase opposite the template base flanking tA*4 on the 3′-side, as well as opposite tA*4, in the case of the 10*S* adduct. Furthermore, this predicts a stalling of the polymerase predominantly opposite the 10*R* adduct. Thus, the differences in the orientations of the BP residue in the 10*S* (+)- and 10*R* (−)-*trans*-*anti*-[BP]-N^6-dA adducts can account for the distinctive stalling patterns observed in the case of T7 DNA polymerase (*47*), and probably other polymerases as well (*78*).

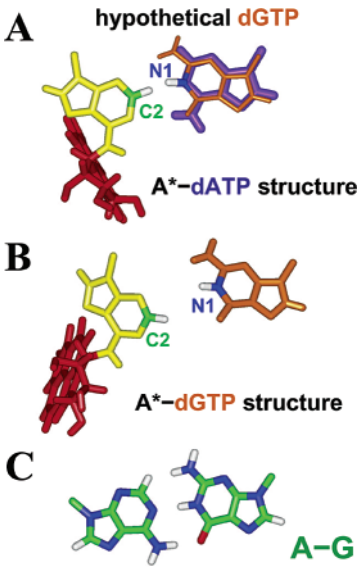

FIGURE 10: Misalignment of the incoming dGTP and the modified template adenine in the tA*4−dGTP structure. (A) tA*4−dATP structure with hypothetical dGTP. (B) tA*4−dGTP structure. (C) Observed *cis* Watson−Crick/Watson−Crick A−G mismatch structure (*73*). BP is in red, and modified adenine is in yellow. dATP is in purple, and dGTP is in orange. N1 and H1 of dGTP, C2 and H2 of modified adenine, and all atoms in (C) are colored by atom type: carbon, green; nitrogen, blue; oxygen, red; hydrogen, white.

Because of the tightness within the active site of the T7 DNA polymerase and the extensive protein−DNA interactions, intercalation of the bulky BP ring system inside the active site is likely to cause serious disruption of crucial polymerase−DNA interactions, which can account for the stalling of polymerases at or near the bulky [BP]-N^6-dA lesion sites. A structure of this type would be expected to cause blockage (see Figure 2). Particularly critical are the minor groove hydrogen bond interactions between conserved protein residues and the primer 3′-terminal base pair, as they are believed to provide a proofreading mechanism to detect mismatches (*51*). The 3′-intercalated BP of the 10*S* (+)-*trans*-*anti*-[BP]-N^6-dA adduct in the active site, occupying the position of the terminal base pair, would totally disrupt these important minor groove hydrogen bond interactions. Such disruptions would be anticipated to both weaken dNTP binding and impede catalysis. The loss of these interactions could stall the polymerase, providing a possible mechanism of polymerase blockage at the lesion site by this adduct.

Also, as revealed by various crystal structures of DNA polymerase complexes (*10*−*15*, *19*), the base immediately 5′ to the templating nucleotide is "flipped out" of the active site by 180°, stacking with a highly conserved aromatic amino acid residue (His607 in this case) (*19*, *51*). This sort of stacking interaction involving His607 and the 5′ base is crucial for normal T7 DNA polymerase replication (*51*). However, with a 10*S* (+)-*trans*-*anti*-[BP]-N^6-dA adduct on the template strand, a putative strong stacking interaction between His607 and the BP aromatic ring system, and only if it is 3′-oriented, might lock the covalently linked template adenine residue from flipping into the active site, a motion that is indispensable for continuing the polymerization cycle. This may account for the observed stalling of the polymerase one base 3′ to the lesion site by this adduct. A model to illustrate this type of structure is shown in Figure 11.

On the other hand, in the case of the 10*R* (−)-*trans*-*anti*-[BP]-N^6-dA adduct, the T7 DNA polymerase is not significantly blocked at the position one base 3′ to the lesion (*47*). Since the BP residue is 5′-oriented with respect to the modified adenine in the 10*R* (−)-*trans*-*anti*-[BP]-N^6-dA adduct, the proposed polymerase-stalling stacking interaction between BP and His607 suggested in the oppositely oriented 10*S* (+)-*trans*-*anti*-[BP]-N^6-dA adduct would not be present, consistent with the experimental observations (*47*).

A−dATP and G*−dATP Mismatches Both Induce Enlargement of the dNTP Base Binding Pocket.* The BP-modified guanine adducts share some properties with their adenine counterparts in terms of their behaviors in T7 DNA polymerase nucleotide incorporation and primer extension assays. Specifically, the 10*S* (+)-*trans*-*anti*-[BP]-N^2-dG adduct also predominantly stalls the T7 DNA polymerase (Sequenase 2.0), as revealed by primer extension experiments (*79*). Also, T7 DNA polymerase preferentially inserts a mismatched dATP opposite a templating BP-modified guanine base when it is stalled (*79*), as it does in the case of the BP-modified adenine (*47*). Previous MD simulations revealed that the modified guanine must assume a *syn* glycosidic conformation with BP in the major groove of the primer−template duplex DNA when the mismatched dATP is incorporated, to avoid destroying crucial protein−DNA interactions on the minor groove side of the primer−template (*80*). This *syn* templating guanine base in the active site of the polymerase permits a mismatched dATP to be accommodated; upon rotation of the guanine to the *syn* glycosidic conformation, the far wall of the dNTP base binding pocket is displaced. This effectively expands the size of the dNTP base binding pocket (*72*). On the other hand, in the case of the BP-modified adenine adducts, the modified template adenine, in the *anti* conformation, is displaced away from the catalytic active site to avoid collisions between the BP ring system and the primer−template DNA (Figures 4B, 5A, and 8B), and this also effectively enlarges the dNTP base binding pocket. In fact, the dNTP base binding pockets in these two cases are quite similar, and both preferentially accommodate a dATP residue, as shown in Figure S10. Moreover, as discussed above, the dynamics average C1′−C1′ distance of the tA*4−dATP mismatch is 11.9 Å within the active site of the T7 DNA polymerase, while it is 12.1 Å in the case of the G*−dATP mismatch (*80*). Thus, the nascent base pairs, tA*4−dATP and G*−dATP, are similarly accommodated in the polymerase active site which can accommodate base pairs with a maximum C1′−C1′ distance of ∼12 Å (*81*, *82*).

CONCLUSIONS

Our MD simulations of the T7 DNA polymerase ternary complexes with a 10*S* (+)-*trans*-*anti*-[BP]-N^6-dA-modified template and all four incoming dNTPs show that the size and shape of the T7 DNA polymerase dNTP binding pocket can be significantly affected by the templating 10*S* (+)-*trans*-*anti*-[BP]-N^6-dA adduct, regardless of the type of incoming dNTP. The modified templating adenine base is displaced away from the active site of the polymerase due to steric hindrance between the BP moiety and the primer−template DNA duplex, which therefore enlarges the dNTP base binding pocket, allowing comfortable accommodation of a mismatched dATP opposite the modified adenine. However,

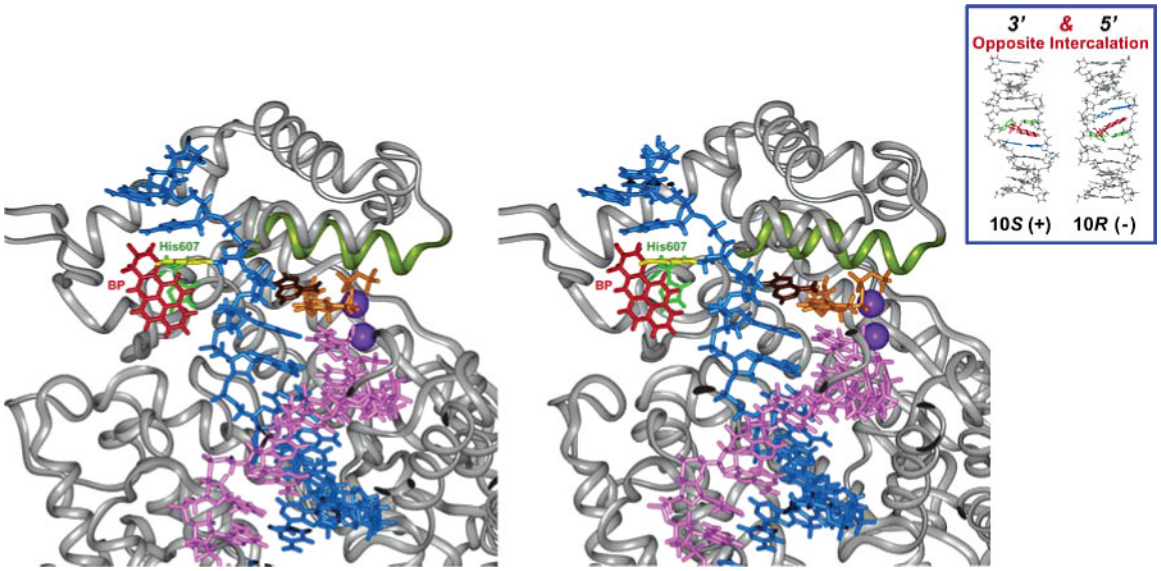

FIGURE 11: Stereoview of a modeled blocking structure of the T7 DNA polymerase complex containing a 10*S* (+) *trans-anti*-[BP]-N^6-dA adduct on the template strand. The protein is in gray ribbon with the O helix in light green. The DNA residues and His607 are in stick. The Mg^{2+} ions are in CPK. The color code is primer, magenta; template, blue; Mg^{2+} ions, purple; dATP, orange; the adenine opposite the incoming dATP, brown; the modified adenine base, yellow; BP, red; His607, green.

this alteration of the dNTP base binding pocket causes poor accommodation of other dNTPs due to imperfect geometric complementarity. These simulations are consistent with nucleotide incorporation experiments that show that dATP is preferably inserted opposite the 10*S* (+)-*trans-anti*-[BP]-N^6-dA lesion (*47*, *83*). Significantly lower extents of insertion of dGTP and dTTP, but not dCTP, by Sequenase 2.0 are also observed (*47*). More generally, our simulations suggesting the influence of bulky adducts on the dNTP base binding pocket could be relevant to other mutagenic bulky adducts in providing a possible structural framework for understanding their influence on polymerase fidelity. Moreover, the general finding that the steric bulk of the adduct on the template causes enlargement of the dNTP base binding pocket is likely to depend little on base sequence context, or the specific high fidelity processive polymerase whose common structural feature is active site tightness in the ternary complex (*72*). The experimental results also show that both the 10*S* (+)- and 10*R* (−)-*trans-anti*-[BP]-N^6-dA adducts block the T7 DNA polymerase; stalling occurs similarly at positions that are one base 3′ to the lesion and at the lesion in the case of the 10*S* (+)-*trans-anti*-[BP]-N^6-dA adduct, while it occurs primarily opposite the lesion in the case of the 10*R* (−)-*trans-anti*-[BP]-N^6-dA adduct. On the basis of stereochemically governed differences of BP adduct orientations, a structural explanation for the different stalling patterns observed in Sequenase 2.0 primer extension experiments with 10*S* (+)- and 10*R* (−)-*trans-anti*-[BP]-N^6-dA adducts in the template strands is proposed.

ACKNOWLEDGMENT

We thank Prof. Robert Shapiro and Dr. Rebecca Perlow for critical reading of the manuscript. Computations were carried out on our own Silicon Graphics Origin 300 server and Octane workstations.

SUPPORTING INFORMATION AVAILABLE

Tables S1−S4 show the partial charges for all four dNTPs. Figure S1 shows the simulation stabilities of both *anti* and *syn* tA*4−dATP structures and the unmodified control. Figure S2 shows the time dependence of χ, α', and β' torsion angles for the *anti* and *syn* tA*4−dATP structures and unmodified control. Figure S3 shows the time dependence of the Cα−N7 distance between Gly527 and template adenine in the *anti* and *syn* tA*4−dATP structures and unmodified control. Figure S4 shows the time dependence of C1′−C1′ distance between the template adenine and incoming dNTP in the *anti* and *syn* tA*4−dATP structures and unmodified control. Figure S5 shows the time dependence of the hydrogen bond distances and angles for the hydrogen bonds involving O9−HO9 hydroxyl group on the benzylic ring and the protein residues Lys536 and Gln539 in the *anti* tA*4−dATP structure. Figure S6 shows the time dependence of the distance between O3′ of the primer termini pT11 and Pα of the incoming dNTP in the *anti* and *syn* tA*4−dATP structures and unmodified control. Figure S7 shows the stereoviews of the active site regions for the simulated T7 DNA polymerase containing tA*4−dTTP, tA*4−dCTP, and tA*4−dGTP, respectively. Figure S8 shows the time dependence of the Cα−N7 distance between Gly527 and template adenine in the tA*4−dTTP, tA*4−dCTP, and tA*4−dGTP structures. Figure S9 shows the stereoviews of the steric hindrance between BP and primer−template DNA in the T7 DNA polymerase with the modified adenine tA*4 *anti* and incoming dTTP, dCTP, and dGTP. Figure S10 shows the stereoviews of the dNTP base binding pockets with the inserted dNTP in the tA*4−dATP and G*−dATP structures. This material is available free of charge via the Internet at http://pubs.acs.org.

REFERENCES

1. Steitz, T. A. (1999) DNA polymerases: structural diversity and common mechanisms, *J. Biol. Chem. 274*, 17395−17398.
2. Doublie, S., Tabor, S., Long, A., Richardson, C., and Ellenberger, T. (1999) An open and closed case for all polymerases, *Structure 7*, R31−R35.
3. Dahlberg, M. E., and Benkovic, S. J. (1991) Kinetic mechanism of DNA polymerase I (Klenow fragment): identification of a second conformational change and evaluation of the internal equilibrium constant, *Biochemistry 30*, 4835−4843.

4. Zhong, X., Patel, S. S., Werneburg, B. G., and Tsai, M. D. (1997) DNA polymerase β: multiple conformational changes in the mechanism of catalysis, *Biochemistry 36*, 11891−11900.
5. Benkovic, S. J., and Cameron, C. E. (1995) Kinetic analysis of nucleotide incorporation and misincorporation by Klenow fragment of *Escherichia coli* DNA polymerase I, *Methods Enzymol. 262*, 257−269.
6. Johnson, K. A. (1993) Conformational coupling in DNA polymerase fidelity, *Annu. Rev. Biochem. 62*, 685−713.
7. Goodman, M. F. (1997) Hydrogen bonding revisited: geometric selection as a principal determinant of DNA replication fidelity, *Proc. Natl. Acad. Sci. U.S.A. 94*, 10493−10495.
8. Echols, H., and Goodman, M. F. (1991) Fidelity mechanisms in DNA replication, *Annu. Rev. Biochem. 60*, 477−511.
9. Kunkel, T. A., and Bebenek, K. (2000) DNA replication fidelity, *Annu. Rev. Biochem. 69*, 497−529.
10. Doublie, S., and Ellenberger, T. (1998) The mechanism of action of T7 DNA polymerase, *Curr. Opin. Struct. Biol. 8*, 704−712.
11. Li, Y., Korolev, S., and Waksman, G. (1998) Crystal structures of open and closed forms of binary and ternary complexes of the large fragment of *Thermus aquaticus* DNA polymerase I: structural basis for nucleotide incorporation, *EMBO J. 17*, 7514−7525.
12. Kiefer, J. R., Mao, C., Braman, J. C., and Beese, L. S. (1998) Visualizing DNA replication in a catalytically active Bacillus DNA polymerase crystal, *Nature 391*, 304−307.
13. Korolev, S., Nayal, M., Barnes, W. M., Di Cera, E., and Waksman, G. (1995) Crystal structure of the large fragment of *Thermus aquaticus* DNA polymerase I at 2.5-angstrom resolution: structural basis for thermostability, *Proc. Natl. Acad. Sci. U.S.A. 92*, 9264−9268.
14. Kim, Y., Eom, S. H., Wang, J., Lee, D. S., Suh, S. W., and Steitz, T. A. (1995) Crystal structure of *Thermus aquaticus* DNA polymerase, *Nature 376*, 612−616.
15. Eom, S. H., Wang, J., and Steitz, T. A. (1996) Structure of *Taq* polymerase with DNA at the polymerase active site, *Nature 382*, 278−281.
16. Sawaya, M. R., Prasad, R., Wilson, S. H., Kraut, J., and Pelletier, H. (1997) Crystal structures of human DNA polymerase beta complexed with gapped and nicked DNA: evidence for an induced fit mechanism, *Biochemistry 36*, 11205−11215.
17. Beese, L. S., Friedman, J. M., and Steitz, T. A. (1993) Crystal structures of the klenow fragment of DNA polymerase I complexed with deoxynucleoside triphosphate and pyrophosphate, *Biochemistry 32*, 14095−14101.
18. Huang, H., Chopra, R., Verdine, G. L., and Harrison, S. C. (1998) Structure of a covalently trapped catalytic complex of HIV-1 reverse transcriptase: implications for drug resistance, *Science 282*, 1669−1675.
19. Patel, P. H., Suzuki, M., Adman, E., Shinkai, A., and Loeb, L. A. (2001) Prokaryotic DNA polymerase I: evolution, structure, and "base flipping" mechanism for nucleotide selection, *J. Mol. Biol. 308*, 823−837.
20. Joyce, C. M., and Steitz, T. A. (1994) Function and structure relationships in DNA polymerases, *Annu. Rev. Biochem. 63*, 777−822.
21. Showalter, A. K., and Tsai, M. D. (2002) A reexamination of the nucleotide incorporation fidelity of DNA polymerases, *Biochemistry 41*, 10571−10576.
22. Florian, J., Goodman, M. F., and Warshel, A. (2003) Computer simulation of the chemical catalysis of DNA polymerases: discriminating between alternative nucleotide insertion mechanisms for T7 DNA polymerase, *J. Am. Chem. Soc. 125*, 8163−8177.
23. Kim, S. J., Beard, W. A., Harvey, J., Shock, D. D., Knutson, J. R., and Wilson, S. H. (2003) Rapid segmental and subdomain motions of DNA polymerase β, *J. Biol. Chem. 278*, 5072−5081.
24. Beard, W. A., and Wilson, S. H. (2003) Structural insights into the origins of DNA polymerase fidelity, *Structure 11*, 489−496.
25. Vande Berg, B. J., Beard, W. A., and Wilson, S. H. (2001) DNA structure and aspartate 276 influence nucleotide binding to human DNA polymerase beta. Implication for the identity of the rate-limiting conformational change, *J. Biol. Chem. 276*, 3408−3416.
26. Yang, L., Beard, W. A., Wilson, S. H., Broyde, S., and Schlick, T. (2002) Polymerase β simulations suggest that Arg258 rotation is a slow step rather than large subdomain motions *per se*, *J. Mol. Biol. 317*, 651−671.
27. Minnick, D. T., Bebenek, K., Osheroff, W. P., Turner, R. M., Astatke, M., Liu, L., Kunkel, T. A., and Joyce, C. M. (1999) Side chains that influence fidelity at the polymerase active site of *Escherichia coli* DNA polymerase I (Klenow fragment), *J. Biol. Chem. 274*, 3067−3075.
28. Phillips, D. H. (1999) Polycyclic aromatic hydrocarbons in the diet, *Mutat. Res. 443*, 139−147.
29. Grimmer, G. (1993) Relevance of polycyclic aromatic hydrocarbons as environmental carcinogens. In *Proc. 13th Int. Symp. Polynuclear Aromatic Hydrocarbons* (Garrigues, P., Lamotte, M., Eds.) pp 31−41, Gordon and Breach Science Publishers, Langhorne, PA.
30. Harvey, R. G. (1991) *Polycyclic Aromatic Hydrocarbons: Chemistry and Carcinogenicity*, Cambridge University Press, Cambridge, UK.
31. Perrin, J., Poirot, N., Liska, P., Hanras, C., Theinpont, A., and Felix, G. (1993) Trace enrichment and HPLC analysis of PAHs in edible oils and fat products, using liquid chromatography on electron acceptor stationary phases and fluorescence detection. In *Proc. 13th Int. Symp. Polynuclear Aromatic Hydrocarbons* (Garrigues, P., Lamotte, M., Eds.), Gordon and Breach Science Publishers, Langhorne, PA.
32. Conney, A. H. (1982) Induction of microsomal enzymes by foreign chemicals and carcinogenesis by polycyclic aromatic hydrocarbons: G. H. A. Clowes Memorial Lecture, *Cancer Res. 42*, 4875−4917.
33. Cheng, S. C., Hilton, B. D., Roman, J. M., and Dipple, A. (1989) DNA adducts from carcinogenic and noncarcinogenic enantiomers of benzo[*a*]pyrene dihydrodiol epoxide, *Chem. Res. Toxicol. 2*, 334−340.
34. Meehan, T., and Straub, K. (1979) Double-stranded DNA stereoselectively binds benzo[*a*]pyrene diol epoxides, *Nature 277*, 410−412.
35. Szeliga, J., and Dipple, A. (1998) DNA adduct formation by polycyclic aromatic hydrocarbon dihydrodiol epoxides, *Chem. Res. Toxicol. 11*, 1−11.
36. Zegar, I. S., Kim, S. J., Johansen, T. N., Horton, P. J., Harris, C. M., Harris, T. M., and Stone, M. P. (1996) Adduction of the human *N-ras* codon 61 sequence with (−)-(7*S*,8*R*,9*R*,10*S*)-7,8-dihydroxy-9,10-epoxy-7,8,9,10-tetrahydrobenzo[*a*] pyrene: structural refinement of the intercalated SRSR(61,2) (−)-(7*S*,8*R*,9*S*,10*R*)-N6-[10-(7,8,9,10-tetrahydrobenzo[*a*]pyrenyl)]-2′-deoxyadenosyl adduct from 1H NMR, *Biochemistry 35*, 6212−6224.
37. Schwartz, J. L., Rice, J. S., Luxon, B. A., Sayer, J. M., Xie, G., Yeh, H. J., Liu, X., Jerina, D. M., and Gorenstein, D. G. (1997) Solution structure of the minor conformer of a DNA duplex containing a dG mismatch opposite a benzo[*a*]pyrene diol epoxide/dA adduct: glycosidic rotation from *syn* to *anti* at the modified deoxyadenosine, *Biochemistry 36*, 11069−11076.
38. Yeh, H. J. C., Sayer, J. M., Liu, X., Altieri, A. S., Byrd, R. A., Lakshman, M. K., Yagi, H., Schurter, E. J., Gorenstein, D. G., and Jerina, D. M. (1995) NMR solution structure of a nonanucleotide duplex with a dG mismatch opposite a 10*S* adduct derived from *trans* addition of a deoxyadenosine N6-amino group to (+)-(7*R*,8*S*,9*S*,10*R*)-7,8-dihydroxy-9,10-epoxy-7,8,9,10-tetrahydrobenzo[*a*]pyrene: an unusual *syn* glycosidic torsion angle at the modified dA, *Biochemistry 34*, 13570−13581.
39. Schurter, E. J., Sayer, J. M., Oh-hara, T., Yeh, H. J. C., Yagi, H., Luxon, B. A., Jerina, D. M., and Gorenstein, D. G. (1995) NMR solution structure of an undecanucleotide duplex with a complementary thymidine base opposite a 10*R* adduct derived from *trans* addition of a deoxyadenosine N6-amino group to (−)-(7*R*,8*S*,9*R*,10*S*)-7,8-dihydroxy-9,10-epoxy-7,8,9,10-tetrahydrobenzo[*a*]pyrene, *Biochemistry 34*, 9009−9020.
40. Pradhan, P., Tirumala, S., Liu, X., Sayer, J. M., Jerina, D. M., and Yeh, H. J. C. (2001) Solution structure of a *trans*-opened (10*S*)-dA adduct of (+)-(7*S*,8*R*,9*S*,10*R*)-7,8-dihydroxy-9,10-epoxy-7,8,9,10-tetrahydrobenzo[*a*]pyrene in a fully complementary DNA duplex: evidence for a major *syn* conformation, *Biochemistry 40*, 5870−5881.
41. Volk, D. E., Rice, J. S., Luxon, B. A., Yeh, H. J. C., Liang, C., Xie, G., Sayer, J. M., Jerina, D. M., and Gorenstein, D. G. (2000) NMR evidence for *syn-anti* interconversion of a *trans* opened (10*R*)-dA adduct of benzo[*a*]pyrene (7*S*,8*R*)-diol (9*R*,10*S*)-epoxide in a DNA duplex, *Biochemistry 39*, 14040−14053.
42. Mao, B., Gu, Z., Gorin, A., Chen, J., Hingerty, B. E., Amin, S., Broyde, S., Geacintov, N. E., and Patel, D. J. (1999) Solution structure of the (+)-*cis-anti*-benzo[*a*]pyrene-dA ([BP]dA) adduct opposite dT in a DNA duplex, *Biochemistry 38*, 10831−10842.
43. Weinberg, R. A. (1996) How cancer arises, *Sci. Am. 275*, 62−70.
44. Garner, R. C. (1998) The role of DNA adducts in chemical carcinogenesis, *Mutat. Res. 402*, 67−75.

45. Wiencke, J. K. (2002) DNA adduct burden and tobacco carcinogenesis, *Oncogene 21*, 7376−7391.
46. Gibbs, W. W. (2003) Untangling the roots of cancer, *Sci. Am. 289*, 56−65.
47. Chary, P., and Lloyd, R. S. (1995) In vitro replication by prokaryotic and eukaryotic polymerases on DNA templates containing site-specific and stereospecific benzo[*a*]pyrene-7,8-dihydrodiol-9,10-epoxide adducts, *Nucleic Acids Res. 23*, 1398−1405.
48. Taylor, J. S. (2002) New structural and mechanistic insight into the A-rule and the instructional and non-instructional behavior of DNA photoproducts and other lesions, *Mutat. Res. 510*, 55−70.
49. Shibutani, S., Takeshita, M., and Grollman, A. P. (1997) Translesional synthesis on DNA templates containing a single abasic site. A mechanistic study of the "A rule", *J. Biol. Chem. 272*, 13916−13922.
50. Reineks, E. Z., and Berdis, A. J. (2004) Evaluating the contribution of base stacking during translesion DNA replication, *Biochemistry 43*, 393−404.
51. Doublie, S., Tabor, S., Long, A., Richardson, C., and Ellenberger, T. (1998) Crystal structure of a bacteriophage T7 DNA replication complex at 2.2-angstrom resolution, *Nature 391*, 231−232.
52. Berman, H. M., Westbrook, J., Feng, Z., Gilliland, G., Bhat, T. N., Weissig, H., Shindyalov, I. N., and Bourne, P. E. (2000) The protein data bank, *Nucleic Acids Res. 28*.
53. Arnott, S., Smith, P. J. C., and Chandrasekaran, R. (1976) *Handbook of Biochemistry and Molecular Biology*, 3rd ed., CRC Press, Cleveland, OH.
54. Case, D. A., Pearlman, D. A., Caldwell, J. W., Cheatham, T. E., III, Ross, W. S., Simmerling, C. L., Darden, T. A., Merz, K. M., Jr., Stanton, R. V., Cheng, A. L., Vincent, J. J., Crowley, M., Tsui, V., Radner, R., Duan, Y., Pitera, J., Massova, I., Seibel, G. L., Singh, U. C., Weiner, P. K., and Kollman, P. A. (1999) *AMBER 6.0*, University of California, San Francisco, CA.
55. Tan, J., Geacintov, N. E., and Broyde S. (2000) Principles governing conformations in stereoisomeric adducts of bay region benzo[*a*]pyrene diol epoxides to adenine in DNA: steric and hydrophobic effects are dominant, *J. Am. Chem. Soc. 122*, 3021−3032.
56. Yan, S., Shapiro, R., Geacintov, N. E., and Broyde, S. (2001) Stereochemical, structural and thermodynamic origins of stability differences between stereoisomeric benzo[*a*]pyrene diol epoxide deoxyadenosine adducts in a DNA mutational hot spot sequence, *J. Am. Chem. Soc. 123*, 7054−7066.
57. Frisch, M. J., Trucks, G. W., Schlegel, H. B., Gill, P., Johnsone, B. G., Robb, M. A., Cheeseman, J. R., Keith, T. A., Petersson, G. A., Montgomery, J. A., Raghavachari, K., Al-Laham, M. A., Zakrzewski, V. G., Ortiz, J. V., Foresman, J. B., Cioslowski, J., Stefanov, B. B., Nanayakkara, A., Challacombe, M., Peng, C. Y., Ayala, P. Y., Chen, W., Wong, M. W., Andres, J. L., Reploge, E. S., Gomperts, R., Martin, R. L., Fox, D. J., Binkley, J. S., Defrees, D. J., Baker, J., Stewart, j. P., Head-Gordon, M., Gonzalez, C., and Pople, J. A. (1995) *Gaussian 94 (Revision A.1)*, Pittsburgh, PA.
58. Bayly, C. I., Cieplak, P., Cornell, W. D., and Kollman, P. A. (1993) A well-behaved electrostatic potential based method using charge restraints for deriving atomic charges: the RESP model, *J. Phys. Chem. 97*, 10269−10280.
59. Cheatham, T. E., III, Cieplak, P., and Kollman, P. A. (1999) A modified version of the Cornell et al. force field with improved sugar pucker phases and helical repeat, *J. Biomol. Struct. Dyn. 16*, 845−862.
60. Darden, T., York, D., and Pedersen, L. (1993) Particle mesh Ewald: an *N* log(*N*) method for Ewald sums in large systems, *J. Chem. Phys. 98*, 10089−10092.
61. Essmann, U., Perera, L., Berkowitz, M. L., Darden, T., Lee, H., and Pederson, L. G. (1995) A smooth particle mesh Ewald method, *J. Chem. Phys. 103*, 8577−8593.
62. Ryckaert, J. P., Ciccotti, G., and Berendsen, H. J. C. (1977) Numerical integration of Cartesian equations of motion of a system with constraints: molecular dynamics of *n*-alkanes, *J. Comput. Phys. 23*, 327−341.
63. Harvey, S. C., Tan, R. K.-Z., and Cheatham, T. E. (1998) The flying ice cube: velocity rescaling in molecular dynamics leads to violation of energy equipartition., *J. Comput. Chem. 19*, 726−740.
64. Jorgensen, W. L., Chandreskhar, J., Madura, J. D., Imprey, R. W., and Klein, M. L. (1983) Comparison of simple potential functions for simulating liquid water, *J. Chem. Phys. 79*, 926−935.
65. Mezei, M. (1997) Optimal position of solute for simulations, *J. Comput. Chem. 18*, 812−815.
66. Berendsen, H. J. C., Postma, J. P. M., van Gunsteren, W. F., DiNola, A., and Haak, J. R. (1984) Molecular dynamics with coupling to an external bath, *J. Chem. Phys. 81*, 3684−3690.
67. Connolly, M. L. (1983) Solvent-accessible surfaces of proteins and nucleic acids, *Science 221*, 709−713.
68. Bruskov, V. I., and Poltev, V. I. (1979) On molecular mechanisms of nucleic acid synthesis. Fidelity aspects: 2. Contribution of protein-nucleotide recognition, *J. Theor. Biol. 78*, 29−41.
69. Engel, J. D., and von Hippel, P. H. (1978) Effects of methylation on the stability of nucleic acid conformations: studies at the polymer level, *J. Biol. Chem. 253*, 927−934.
70. Sloane, D. L., Goodman, M. F., and Echols, H. (1988) The fidelity of base selection by the polymerase subunit of DNA polymerase III holoenzyme, *Nucleic Acids Res. 16*, 6465−6475.
71. Kool, E. T. (2001) Hydrogen bonding, base stacking, and steric effects in DNA replication, *Annu. Rev. Biophys. Biomol. Struct. 30*, 1−22.
72. Kool, E. T. (2002) Active site tightness and substrate fit in DNA replication, *Annu. Rev. Biochem. 71*, 191−219.
73. Leontis, N. B., Stombaugh, J., and Westhof, E. (2002) The non-Watson−Crick base pairs and their associated isostericity matrices, *Nucleic Acids Res. 30*, 3497−3531.
74. Steitz, T. A. (1998) A mechanism for all polymerases, *Nature 391*, 231−232.
75. Steitz, T. A. (1993) DNA-dependent and RNA-dependent DNA polymerases, *Curr. Opin. Struct. Biol. 3*, 31−38.
76. Wong, I., Patel, S. S., and Johnson, K. A. (1991) An induced-fit kinetic mechanism for DNA replication fidelity: direct measurement by single-turnover kinetics, *Biochemistry 30*, 526−537.
77. Patel, S. S., Wong, I., and Johnson, K. A. (1991) Pre-steady-state kinetic analysis of processive DNA replication including complete characterization of an exonuclease-deficient mutant, *Biochemistry 30*, 511−525.
78. Christner, D. F., Lakshman, M. K., Sayer, J. M., Jerina, D. M., and Dipple, A. (1994) Primer extension by various polymerases using oligonucleotide templates containing stereoisomeric benzo-[*a*]pyrene-deoxyadenosine adducts, *Biochemistry 33*, 14297−14305.
79. Zhuang, P., Kolbanovskiy, A., Amin, S., and Geacintov, N. E. (2001) Base sequence dependence of in vitro translesional DNA replication past a bulky lesion catalyzed by the exo$^-$ Klenow fragment of Pol I, *Biochemistry 40*, 6660−6669.
80. Perlow, R. A., and Broyde, S. (2001) Evading the proofreading machinery of a replicative DNA polymerase: induction of a mutation by an environmental carcinogen, *J. Mol. Biol. 309*, 519−536.
81. Morales, J., and Kool, E. T. (1998) Efficient replication between non-hydrogen-bonded nucleoside shape analogs, *Nat. Struct. Biol. 5*, 950−954.
82. Barsky, D., Kool, E. T., and Colvin, M. E. (1999) Interaction and solvation energies of nonpolar DNA base analogues and their role in polymerase insertion fidelity, *J. Biomol. Struct. Dyn. 16*, 1119−1134.
83. Zang, H., Guengerich, F. P., and Harris, T. M. (2003) Effect of bound carcinogens on DNA misincorporation kinetics catalyzed by DNA polymerases, *Abstr. Pap. Am. Chem. S. 226*, 65-TOXI.
84. Simmerling, C., Elber, R., and Zhang, J. (1995) MOIL-View − a program for visualization of structure and dynamics of biomolecules and STO − a program for computing stochastic paths. In *Modelling of Biomolecular Structure and Mechanisms* (Pullman, A., Jortner, J., Pullman, B., Eds.) pp 241−265, Kluwer, Netherlands.

BI0499516